3D Modeling of a foreland fold and thrust basin in the French sub-Alpine chains

by

Jules Blom

in partial fulfillment of the requirements for the degree of

Bachelor of Science
in Applied Earth Sciences

at the Delft University of Technology
6 November 2017

Student number: 4319508
Supervisors: Jan Kees Blom & Pierre-Olivier Bruna

TU Delft Delft University of Technology

Abstract

A three-dimensional geological model has been constructed of a 49 square km area in the sub-Alpine chains in the French Drome department. The area was situated in the Vocontian Basin, which was an epicontinental sea situated at the western margin of the Alpine Tethys Ocean, between former continents of Gondwana and Laurasia. Formations of limestones and marls have been deposited over a time span of approximately 80 Ma from the Late Jurassic to the Early Cretaceous, which can be classified into eight distinct formations. This was followed by two phases of deformation. First, the counter-clockwise rotation of Iberia into Europe inducing S-N compression in this area. Second, the collision of Adria with the European continent inducing E-W compression. Both events uplifted the area by an estimated 2500 to 3000 m.

This thesis uses data collected during the second year fieldwork (course AESB2430) of the Applied Earth Sciences bachelor at Delft University of Technology. The cross sections and geological map from this fieldwork were revised where necessary. Three new cross-sections were constructed along the north, east, and west boundaries of the area for more coverage. All cross-sections were digitized using the Move software package. To check whether these were geologically feasible, they were restored to their pre-deformation state by removing the effect of faulting and folding. These cross-sections form the basis for a 1:25 000 scale three-dimensional model. Horizon surfaces were created between cross-section horizons using spline interpolation and fault surfaces using linear interpolation

Fauld displacements are removed and an unfolding is performed on the 3D model, in an attempt to reconstruct a balanced pre-deformational setting. The result is a viable model, with some inaccuracies such as gaps and overlaps between formation surfaces and slight variation s in layer thickness. The aim of this 3D model is to aid the understanding of the configuration of rocks and of the structural evolution of the area. The average shortening due to deformation for cross-sections was found to be 14.71 %. The surface reduction value of the area is found to be 8.2 km^2 or 14.3 %.

The direction of shortening is primarily in the S-N, due to the Iberian collision, and to lesser extent in the E-W direction, due to the Adriatic collision.

Contents

1

Introduction

The goal of this thesis is to produce a geologically feasible three-dimensional model of the Montagne de Banne area using the Move software package in order to visualize and understand the distribution of the formations in the subsurface and to better understand the structural evolution of the area.

This thesis uses data collected during the fieldwork to the Montagne de Banne area for the course AESB2430 of the Applied Earth Sciences bachelor at Delft University of Technology. Montagne de Banne is situated in the Sub-Alpine chains in the Nyons Arrondissement in the Drôme Department in the South East of France. The Sub-Alpine chains are a typical fold-and-thrust mountain chain. During this fieldwork, observations were made to construct several cross-sections and a geological map of the area.

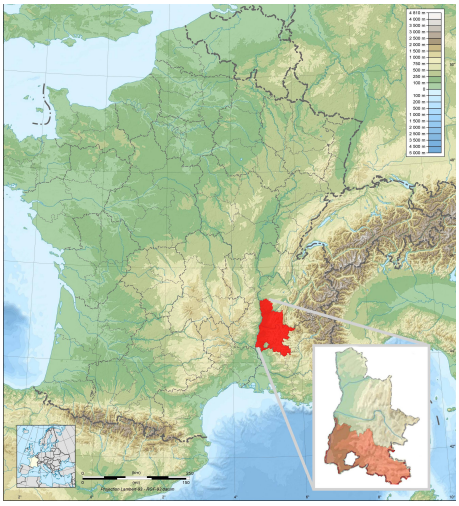

Figure 1.1: Location of Nyons arrondissement in France

First, a digital elevation model is made in the Move software suite, provided by Midland Valley Ltd. Move suite is a structural modeling and analysis toolkit. It provides a full georeferenced environment for structural modeling and for integrating and interpreting data, cross-section construction, 3D model building, kinematic restoration and validation (Mov, 2017).

The cross-sections made during the fieldwork are reviewed and revised where necessary. New cross-sections are constructed for more coverage of the area. All cross-sections are digitized into the Move suite software package.

The cross-sections are restored by means of moving the formation horizons along the faults and unfolding with a kinematic algorithm assuming a flexural-slip folding mechanism. By moving the faults back into place any discrepancies in layer thickness or dip are exposed. By unfolding the cross-sections unaccounted variations in length and thickness are revealed. Finally, section analysis is used to validate the horizons lengths.

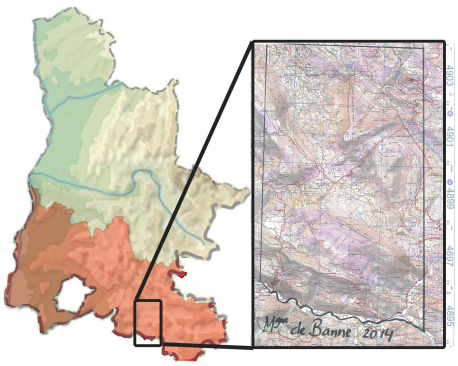

Figure 1.2: Location of studied area in Nyons arrondissement

Once all the restored cross-sections no longer have unaccountable changes in area or length then they can be considered 'balanced' meaning that the interpretation is geologically possible.

These cross-sections form the basis for a 3D model. The 3D formation horizons are constructed using spline interpolation between the cross-sections formation horizons. Lin-

ear interpolation is used for the fault surfaces. Fault dis-
placements were removed in the 3D model and the 3D surfaces were unfolded. Any apparent errors emerging from the reconstruction, such as gaps and overlaps between the surfaces, were corrected. The end result should be a viable 3D model.

2

Geological History

Knowledge of the geologic history of the area is key for understanding its present configuration and its structural evolution. Depositional conditions will be described for each formation found in the studied area.

The time of sediment deposition in the studied area spans from the Late Jurassic Oxfordian (ca. 163.5 Ma) to the Early Cretaceous Albian (ca. 100.5 Ma) (Lemoine and Bas, 1986), (M. Wilpshaar et al, 1997). This was followed by two phases of deformation starting in the Late Cretaceous and continuing until present (Lemoine and Bas, 1986).

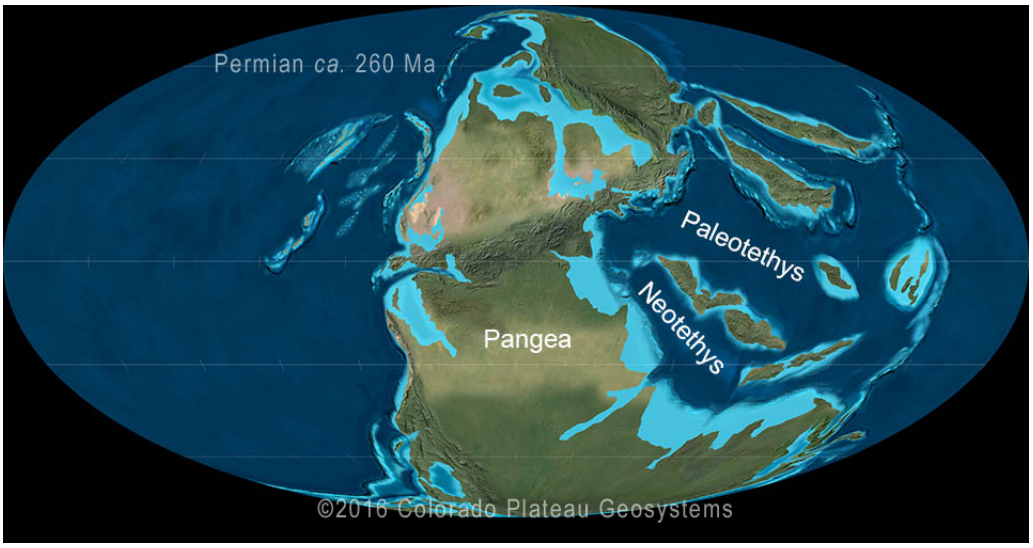

Figure 2.1: Paleogeography in Permian (260 ma) From: Colorado Plateau Geosystems

At the end of the Permian (ca. 252 Ma) all continents were clustered into a supercontinent named Pangea (Lemoine and Bas, 1986). Rifting, starting in the Triassic, the split Pangea into two new supercontinents, Gondwana in the north and Laurasia in the south (Ranging *et al.*, 2010). In Triassic times the studied area appeared as an evaporite basin (Courjault et al, 2011). Diapirism occurs at fault intersections in the greater area, however no Triassic deposits surface in the studied area (P. Joseph et al, 1989). A large, elongate pull-apart basin formed in between Gondwana and Laurasia from the Early to Middle-Jurassic. A subsequent oceanic spreading phase resulted in the opening of the oceanic segment separating the European and Adriatic continental plates (roughly modern day Italy) (M. Wilpshaar et al, 1997). This segment was part of the Mesozoic Tethys Ocean and is called the Alpine Tethys, or the Piedmonte-Ligurian Ocean (M. Wilpshaar et al, 1997). Alpine Tethys was a shallow tropical sea with fluctuating sea levels (Lemoine and Bas, 1986). This rifting stage lasted up to 40 Ma and was not uniform in rate (Lemoine and Bas, 1986).

In isostatic response to to crustal thinning, the passive margin of Alpine Tethys subsided rapidly during the Middle and Late Jurassic, creating the Dauphinois, or French sub-Alpine, Basin (M. Wilpshaar et al, 1997). A deeper part of this basin along the north-western margin of the Alpine Tethys is called the Vocontian Basin, which the area described in this report was situated in (Bombardiere and Gorin, 2000).

During the Late Jurassic and Early Cretaceous the Vocontian Basin was bounded by stable carbonate platforms to the north and south. These were the Jura and Vercors platforms to the north and the Provence platform to the south (Bombardiere and Gorin, 2000), (M. Wilpshaar et al, 1997). See 2.2 for a map showing the paleogeography of the Vocontian Basin and surrounding carbonate platforms in the Valanginian. These carbonate platforms were flanked by mountain ranges, the Corse-Sardaigne Massif to the south, the Central Massif to the west, the Vosgues-Black Forest to the north and the Brabant–Rhenish–Bohemia chain to the north-east. These emerged lands were the source for large amounts of siliciclastic sediments to the Vocontian basin. The Vocontian Basin is thus characterized by mixed carbonate- siliciclastic sedimentation illustrated by typical marl–limestone couplets. (Greselel & Pettet, 2010)

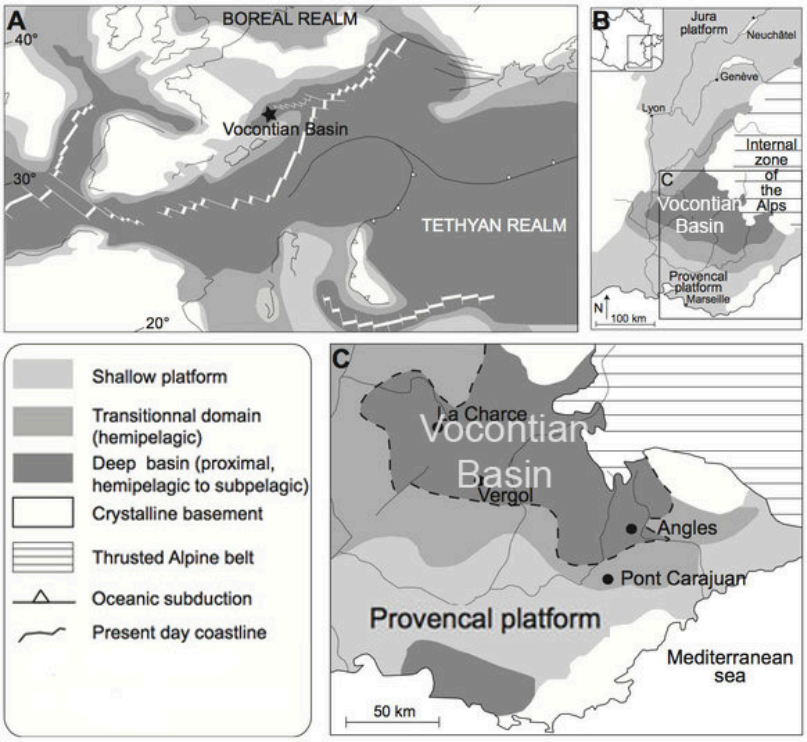

Figure 2.2: Geographic and geologic setting of the Vocontian Basin in the Valanginian (ca 135 Ma). Adapted from Charbonnier (2013)

Continued extensional tectonics during the Middle and Late Jurassic was related to the opening of the Tethyan ocean and possibly northern Atlantic rifting (Boulila et al., 2010). Therefore, throughout the late Jurasssic the area was characterised by many horst and graben structures. The extension lead to an increased deposition of limestones by turbidites and debris flows. (Bombardiere and Gorin, 2000)

The early Oxfordian was a time of cooling associated with a global carbonate production crisis subsidence rates were at its highest of the Late Jurassic (Boulila et al., 2010). Hence from the Early to Middle Oxfordian several hundred meters of pelagic marls accumulated in suboxic conditions in the Vocontian Basin (Breheret and H.J., 2000). This formation, named the Terres Noires formation, is very dark in colour and erodes easily.

In the late Oxfordian carbonate platforms around the margins of the basin expanded and more pelagic limestone layers were deposited (Boulila et al., 2010).

Both the Kimmeridgian and Tithonian deposits form a thick marl–limestone succession, prograding from the inner shelf-barrier domain to the outer mud-dominated shelf (Micarelli et al., 2005).

In the Kimmeridgian well-bedded limestones alternating with thin marlstone interbeds were deposited (Courjault et al, 2011). With most limestones being pelagic to hemipelagic mud- or wackestones (Bombardiere and Gorin, 2000).

During lowstand periods, carbonate production shifts basinwards and the terrigenous input of clay increases. Rapid progradation can lead to oversteepening of slopes and to slump deposits. (Haq 1991 as cited in (Bombardiere and Gorin, 2000)). Hence upper Kimmeridgian to lower Berriasian deposits are riddled with breccias and slump deposits. (Courjault et al, 2011)

Rifting was at its peak in the Tithonian. This tectonic activity was at the origin of increased debris

flows. These debris flows originated from the carbonate shelf and roughly followed fault structures in the continental slope. Because of these depositional mechanisms, the formation thickness can vary within the region (Courjault et al, 2011). The result is a 20–200-m-thick cliff-forming limestone in the centre of the basin (Micarelli et al., 2005). The resistance to erosion makes this formation an easy reference level in the landscape.

Subsidence rates decreased in the Berrassian but irregular limestone deposits from the Berrassian still suggest turbulent conditions in this period. Oversteepening of slopes led to turbidite deposits, which are interposed by pelagic marls (Courjault et al, 2011).

During the Valanginian and Hauterivian the rate of tectonic subsidence in the Dauphinois Basin was relatively uniform. The basin attained its maximum depth (500 - 800 m) around this time (Mattioli *et al.*, 2008). The Early to Late Valanginian transition was marked by a pronounced episode of carbonate platform caused by global climactic change. This crisis combined with sea-level highstand lead to increased marl deposition relative to limestone (Greselel & Pettet, 2010). The sediments from the Valanginian and Hauterivian exhibit very regular marl–limestone alternations. These couplets were formed under the climactic influence of the precession cycle i.e. the wobbling of the Earth about its axis of rotation like a spinning toll (Boulila et al., 2015). This wobbling causes changes in global climate and therefore changes in sea levels (Boulila et al., 2010). This in turn caused changes in the type of sediments deposited. The duration of one such climactic precession cycle is approximately 21 000 years (Colombié and Strasser, 2004).

During the Barremian relatively rapid tectonic uplift large took plate, lifting shallower areas of the margin of the basin into the euphotic zone creating ideal shallow marine carbonate platform environments. Consequently, extensive carbonate platforms formed on the margins of the Vocontian Basin. This could occur on a large scale because the Vocontian Basin was at most only a few hundred metres deep during the Early Cretaceous (M. Wilpshaar et al, 1997). Rapid progradation lead to oversteepening of slopes and lead to debris flows into the basin. A very hard limestone formation with chert nodules was deposited during the Barremian (Leonide et al, 2012).

During the Late Barremian to early Early Aptian the Dauphinois Basin subsided again. The growth of the carbonate platforms was sustained with the subsidence and the platforms prograded into the Vocontian Basin. The effect of platform progradation resulted in increased deposition of mass-transported sediments in the Vocontian Basin. This was followed by a prolonged period of sea-level lowstand. (M. Wilpshaar et al, 1997)

In response to the onset of a compressional regime in the Mediterranean the deposits changed from carbonate-dominated sediments to more terrigenous-dominated sediments in the Aptian (M. Wilpshaar et al, 1997). The Aptian succession consists of marl and marly calcareous pelagic slope facies. During the late Early-Aptian to Middle-Aptian the Vocontian Basin subsided again. This process created an increased tilting of the area with slope angles allowing a range of gravity-driven deposits such as slumps, turbidite packages and massive sandstones into the basin . The massive sandstones were deposited by high-density turbidity currents (Fries and Parize, 2003).

During the Late Aptian–Albian the subsidence or uplift rates were relatively low and siliciclastic sedimentation prevailed. Uplift of the margins coincided with increased exposure of terrigenous sources in the hinterland. Terrigenous sediment eventually filled the Vocontian Basin because sedimentation exceeded the rate of subsidence. The terrigenous influx terminated large-scale shallow marine carbonate production (M. Wilpshaar et al, 1997). This thick monotonous succession of dark marlstone is called the 'Marnes Bleues' (Koessler et al., 2001). The darkblue color of the Albian-Aptian marls developed as a consequence of organic matter breakdown during early burial. This breakdown uses up oxygen and then proceeds to drive the system to suboxic, sulphate-reducing and ultimately methanogenic conditions (Froelich *et al.*, 1979).

Except for some minor fluvial deposits, no younger formations than the Albian formation are found in the studied area. (Monier *et al.*, 1987)

2.1. Stratigraphy

Pelagic, hemipelagic marls and carbonates and gravity driven carbonates have been deposited over a time span of 63 Ma, from the Oxfordian to the Albian with of thickness of around 1500 m (Courjault et al, 2011). These are subdivided into nine formations based on their lithologies.

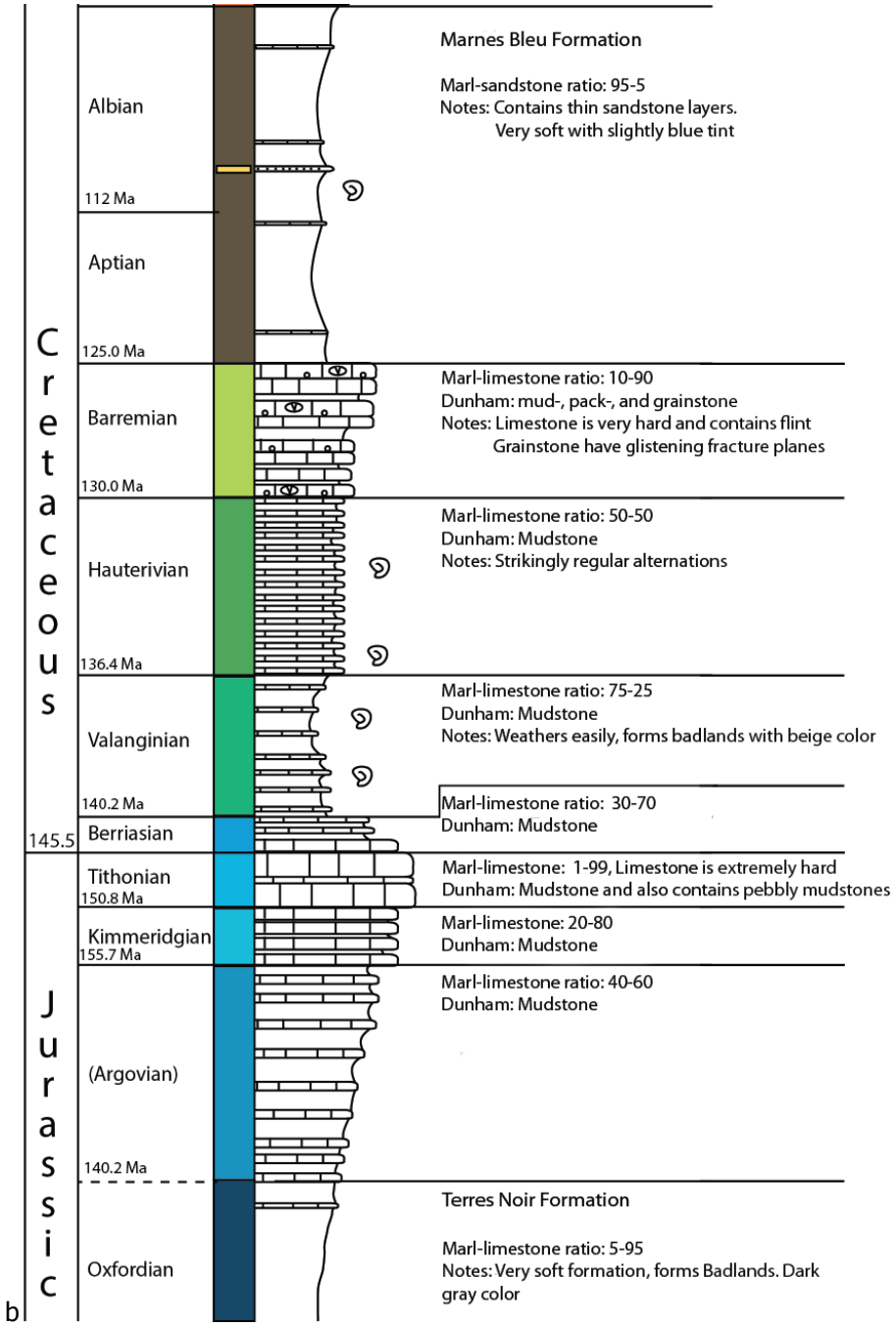

Figure 2.3: Stratigraphic column for deposits found in area. Adapted from Jan Kees Blom's stratigraphic column

2.2. Tectonics

Two distinct phases of deformation can be recognized in the area.

The first phase is the collision of the Iberian Peninsula with the European continent. The opening of the Pyrenean rift system started in Late Jurassic times when Iberia was detached from Newfoundland (Stampfli and Marchant, 2002). From the middle Cretaceous (ca. 110 ma) onward Iberia began to move eastward due the opening of both the Bay of Biscay and the North Atlantic (Stampfli and Marchant, 2002). Iberia rotated into the south of France creating the Pyrenees mountains (Coward and Dietrich, 1989) This collision induced S-to-N oriented compression. This pushed the thick limestones deposited on the Provence platform against the sediments deposited by the Vocontian Basin north (see 2.2 for a schematic map of the Vocontian Basin and the Provence Platform). Shortening in the area occurred over various incompetent detachment horizons to accommodate slip. For example the soft Terres Noires formation, but the Triassic evaporites are the principal and most efficient detachment horizon (Ranging *et al.*, 2010). See 2.5 for a schematic illustration of this phenomenon. The rotation of Iberia ended in the Miocene (Coward and Dietrich, 1989). The S-N oriented compression is also evident from the N-S oriented slope dips in the area.

The second phase, the Alpine orogeny, resulted from the collision of the Adriatic microplate with the European continental margin of the Alpine Tethys ocean during Early Cenozoic times. The Adriatic microplate consisted primarily of continental crust split off from the African plate. This phase is ongoing until present day (Dumont et al., 2011). The formation of compressional structures with a general E-W trend in South-East France resulted from this collision.

Both tectonic events caused uplift of an estimated 2500 - 3000 m in the area.

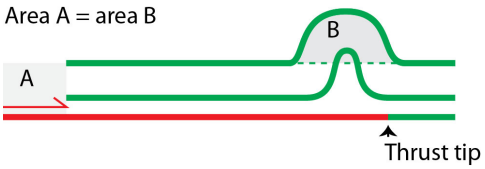

Figure 2.5: Schematic illustration of a detachment fold. The décollement surface is marked red. The thrust tip point in the subsurface is the point beyond which displacement is zero. From John W.F. Waldron

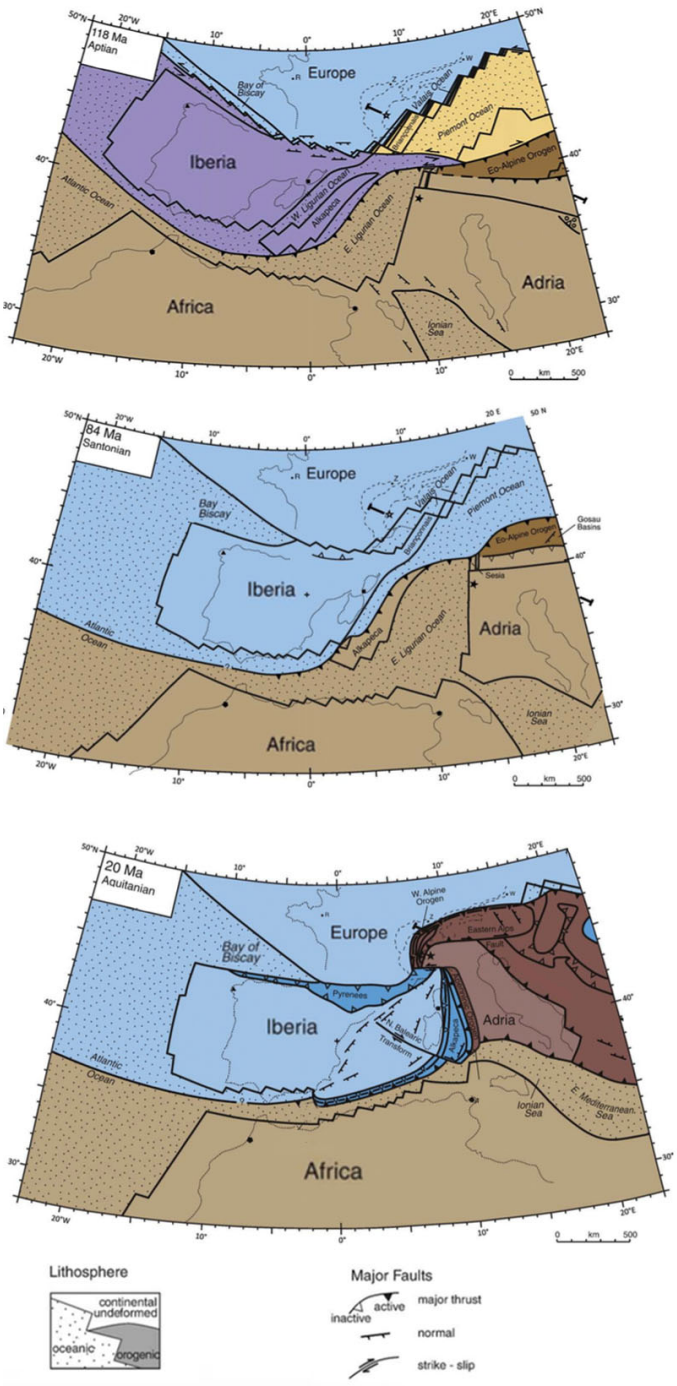

Figure 2.4: Tectonic evolution of SW-Europe from Aptian (119 Ma to Aquitanian 20 Ma). Adapted from M.R. Handy et al. 2010

3

Data

3.1. Digital Elevation Model

A comma-separated file containing the coordinates and elevation of the area was provided. This data was derived from the Shuttle Radar Topography Mission Digital Elevation model and has a resolution of 90m, meaning one datapoint represents 90 m^2. The data was filtered to include only values for the area described in this report. This data was used to construct a digital elevation model in the Move software package. See figure 3.1b below for the result.

North	44°15'60.00
East	5°24'5.55
South	44°10'57.00
West	5°19'26.80

Table 3.1: UTM coordinates of area boundaries

3.2. Fieldwork data

Cross-sections produced during the fieldwork were used. Both the vertical and horizontal axes are 1:25 000 scale. While the cross-section generally contained the main geologic features they were inaccurate in some areas. For example, formation thickness was not really considered in construction. The shape of folds was also often somewhat inaccurate. The way cross-section cross geologic structures should also be taken into account. If a cross-section doesn't cross through a fold perpendicularly then the fold may appear longer than it actually is.

See appendix A for the geological map with locations of cross-section.

New cross-sections were constructed along the north, east and west boundary to be able to create 3D horizons that extend to the boundary of the area.

Two new cross-sections were constructed along the eastern and western extent of the strike-slip fault in order to extend the horizon surfaces up to the face of the

Figure 3.2: Legend for drawn cross-sections

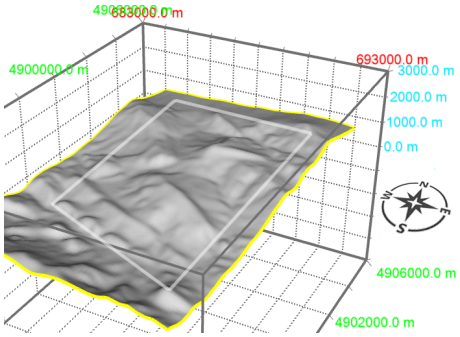

(a) a: DEM with only relief shading

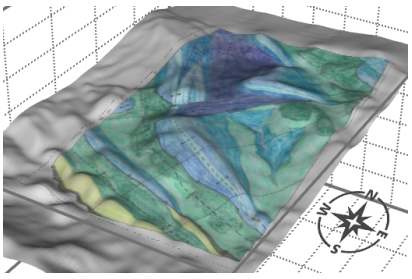

(b) b: DEM with relief shading and draped geological map

Figure 3.1: Digital Elevation Model

fault. These are slightly edited horizon lines from cross-sections 2, 3 and 4.

3.2.1. Cross-sections

Cross-section I

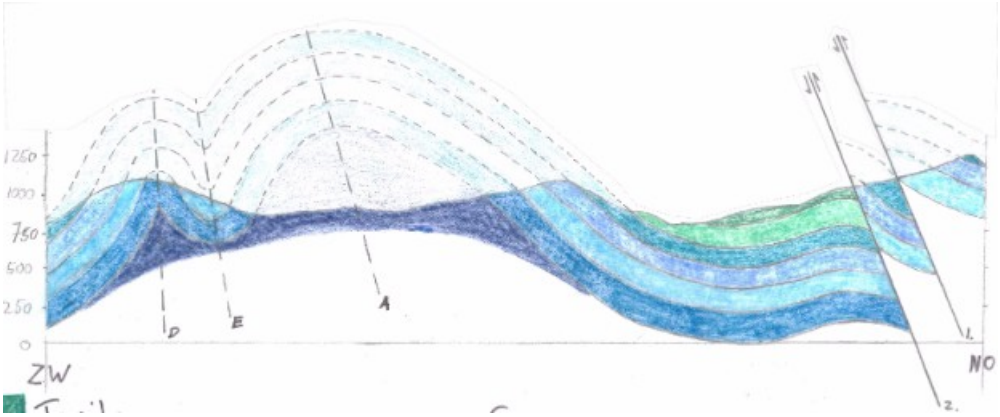

Cross-section II

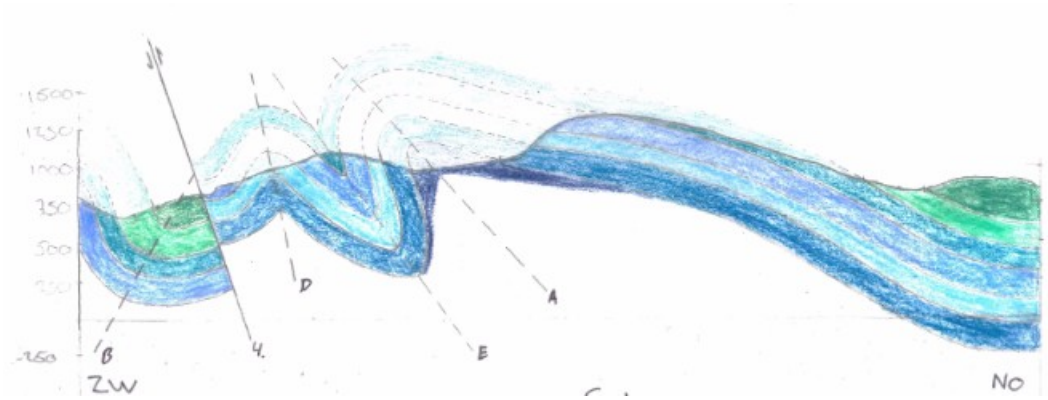

Cross-section III

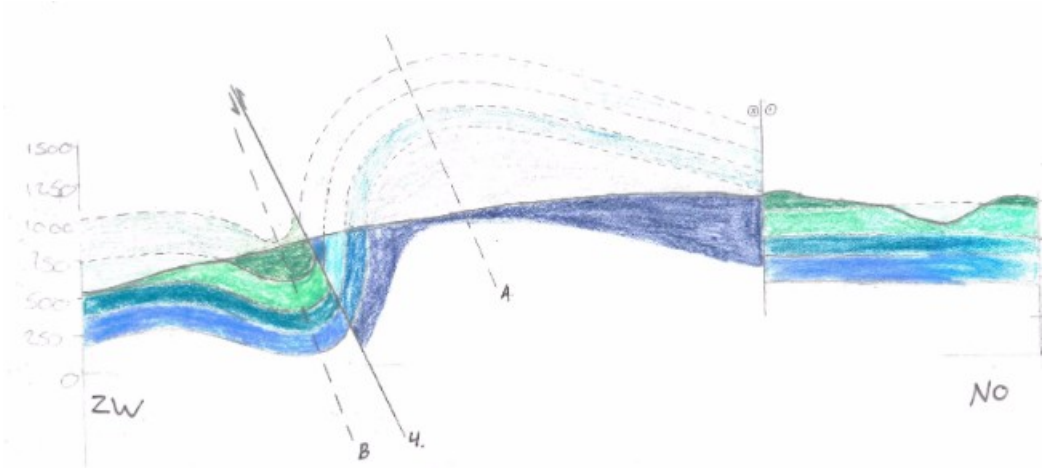

Cross-section IV

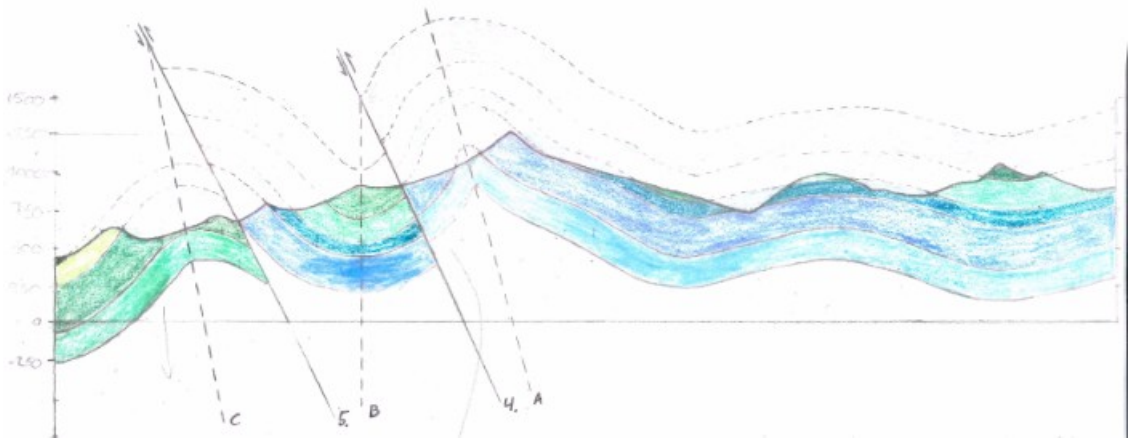

Cross-section V

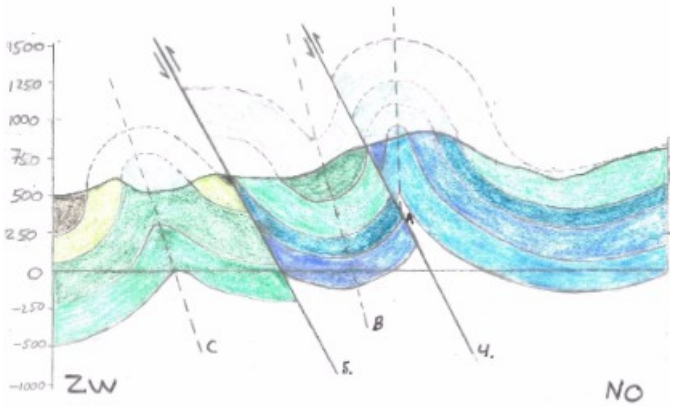

3.2.2. Geological Map

The geological map constructed during the fieldwork was used as the primary source for outcrop, fold and fault locations. See 3.3 for the locations of measured outcrops used to construct this map. In addition, the Vaison-la-Romaine (sheet no. 3140) geological map produced by the BGRM (the French geological survey) was used. This map was also used to view outcrops and geologic structures just outside of the studied area. This map, unfortunately, does not indicate folds and the faults displayed on it are often imprecise. Both maps are included in the appendix.

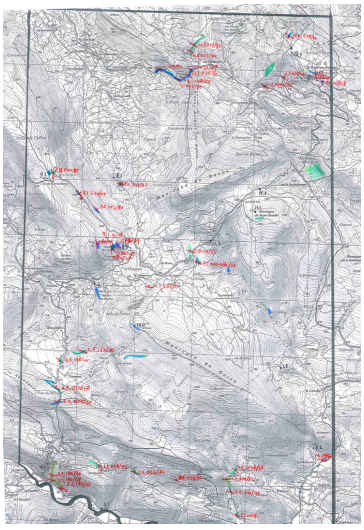

Figure 3.3: Locations of outcrop measurements in 2015 Fieldwork

Google Earth

Google Earth satellite and Street View images were used to view outcrops for additional observations and verification of the geological map. Google Earth also provides the feature to drape an image over the elevated satellite imagery in Google Earth. This comes in very useful for referencing exact outcrop boundaries. Especially very hard formations, such as the Tithonian or Barremian, form characteristic ridges which are easily detectable in satellite images. Conversely, very 'soft' formations, such Valanginian or Lower Oxfordian, also form very recognizable badlands. Figure 3.4 on the next page gives two clear examples of recognizable formations.

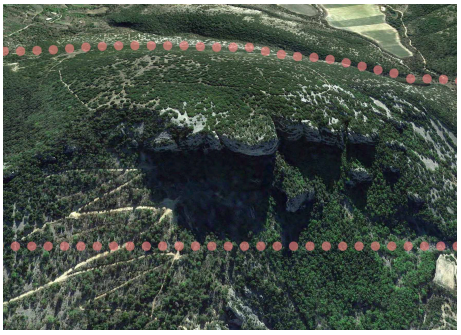

(a) Typical Tithonian formation surfacing in Google Earth satellite image. Approximate formation boundaries marked with dotted line

(b) Unmistakable Valanginian formation badlands

Figure 3.4: Example of recognizable formations in satellite images

3.3. Interpretation from Fieldwork

The following geological map of the area was constructed for the 2015 fieldwork. Faults are assigned numbers, folds letters and cross-sections roman numerals. See the appendix for a larger version of this map.

In fold-and-thrust belts, fold axes are usually perpendicular to the transport direction (John W.F. Waldron). Because the fold axes in the area are mostly E-W, they are thought to have formed during the collision of the Iberia into Europe, which induced compression with a S-N trend in this area. Afterwards, with enduring compression, the reverse-faults formed.

Because folding and thrusting are closely linked in thrust belts, it's quite common for an originally low-angle fault to be rotated either into a steep orientation (John W.F. Waldron). As is the case in this area, with fault dips up to approximately 80°.

The large reverse-fault in the middle and the folds north of it are suspected to owe their SW-NE orientation to the E-W oriented compression induced by the Alpine oregony. The strike-slip faults are also suspected to originate in the Alpine Oregony. The strike-slip faults terminate against the reverse-fault (fault 4), this type of fault is called a tranfer fault. Transfer faults are strike-slip faults that transfer displacement from one fault to another. Transfer faults are therefore bounded and cannot grow freely, which has implications for their displacement–length relations. (Haakon Fossen, 2010)

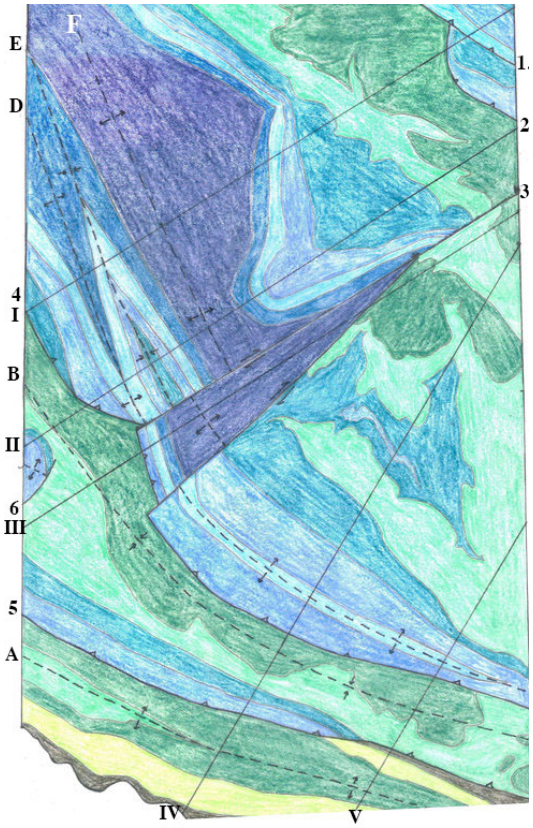

Figure 3.5: Geologic Map from 2015 fieldwork

4

2D Modelling

4.1. Digitizing cross-sections

The first step is digitizing the existing cross-sections. This is done in the following order.

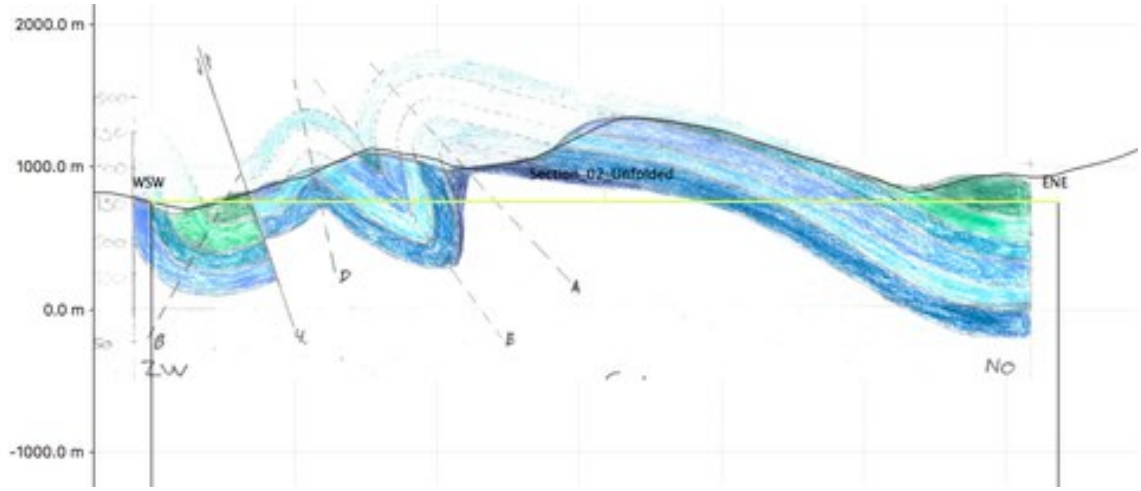

Figure 4.1: Cross-section II from fieldwork inserted and calibrated in cross-section into Move software

1. Stratigraphy is defined in Move for assigning properties during horizon creation
2. Exact cross-section locations are traced in Move
3. Altitude profiles are collected from the Digital Elevation Model for each cross-section
4. The scanned images of drawn cross-section are added and their locations calibrated.
5. Horizons traced from the images and adjusted where necessary
6. Where necessary B-spline resampling is applied to smooth the traced line.

4.2. Restoration

Deformation is assumed to neither create nor destroy rock volume. Therefore it should be possible to obtain the undeformed state by undoing the effects of faulting and folding. (Mov, 2017)

Section balancing is the validation of an interpretation through restoration to a depositional, pre-deformational state achieved by applying certain geometric rules (Mov, 2017).

This involves removing the effects of fault displacements and folding associated with flexural slip. Volume loss due to erosion and compaction are not considered in this thesis.

[H]

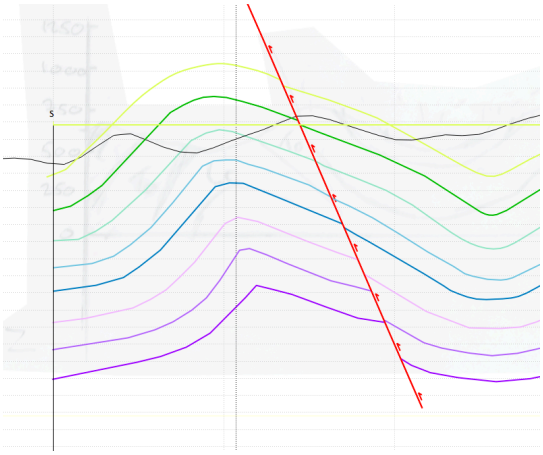

(a) Example of problematic moved-on-fault cross-section

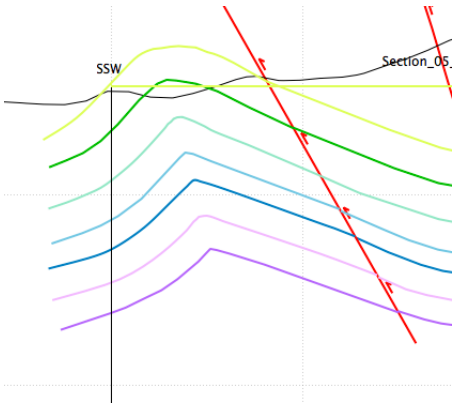

(b) Corrected moved-on-fault cross-section

Figure 4.2: Adjusting cross-section by removing fault displacement

It should be noted that a balanced cross-section does not necessarily reflect correctness and is not a unique solution. It merely indicates that the present interpretation is a geologically viable one. (Haakon Fossen, 2010)

4.2.1. Removing fault displacement

For restoration purposes, it is assumed that folding took place completely before faulting. Therefore the first step of restoration is moving formations 'back into place' along fault surfaces. This is performed to uncover any differences in thickness, any 'unnaturally' oblique angles or small gaps between horizons. These are subsequently corrected.

The algorithm to remove the fault displacements is called fault-parallel flow. This is a kinematic restoration algorithm especially developed for moving geologic bodies along faults. Fault-parallel flow is a scale-independent method describing how material nodes are displaced parallel to the fault plane, in the direction of fault movement (Ziesch, 2014).

A hanging- and a foot wall of the same formation have to be selected. The algorithm will use these to to calculate the distance of fault displacement and join the horizons.

4.2.2. Unfolding

Flexural-Slip Unfolding

Flexural-slip is the assumed mechanism of folding. Flexural slip implies slip along layer interfaces during folding.

A simple analogy often used to visualize flexural slip is folding double sandwiches with jelly in between. The sandwich maintains its thickness even though slip occurs between the pieces of bread, until the fold becomes too tight. It is a prerequisite for flexural slip that the deforming medium is layered or has a strong mechanical anisotropy (Haakon Fossen, 2010).

Flexural slip unfolding is used because it maintains bed thickness variations and line length is maintained in passive objects that are parallel to the template beds (Mov, 2017).

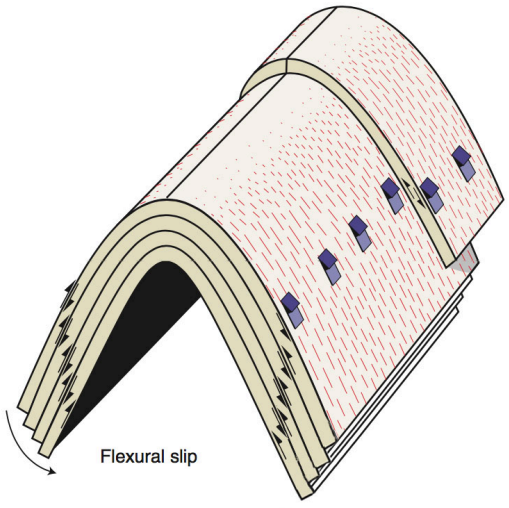

Figure 4.3: Flexural Slip Folding showing opposite sense of slip on each limb, decreasing towards the hinge zone. From Fossen Structural Geology

The unfolding algorithm works by rotating the limbs of a fold to a template bed. Layer parallel shear is then applied to the rotated fold limbs in order to remove the effects of the flexural-slip component of folding. A 'pin' line perpendicular to all horizons is required to indicate the location of no slip. The pin should correspond to the axial surface of the fold (Mov, 2017).

The horizon that is most 'certain' is chosen as the template bed for unfolding. In practice this is always the formation that surfaces most in the cross-section. Formations farther from the surface are somewhat estimated and therefore less suitable as template beds.

Harder formation, like the Tithonian or Barremian formations, are more resistant to erosion and hence maintain shape more than softer formations. Softer formations, i.e. those with a high marl content like Terres Noires or the Valanginian, tend to fold more in a more viscous manner. Accordingly, these harder formations are also preferred as template beds.

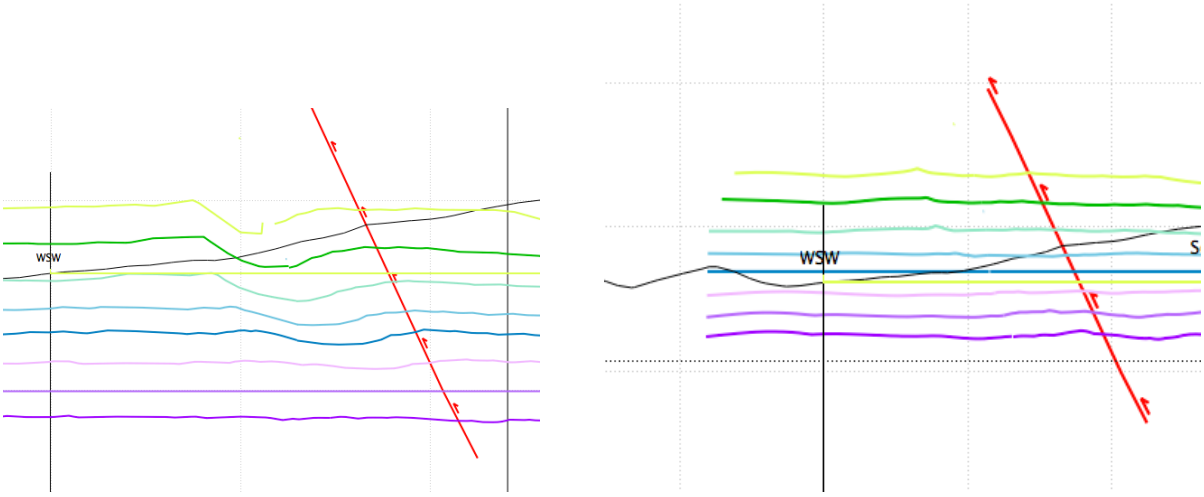

(a) Example of change in bed thickness in hinge zone of cross-section 3 after flexural-unfolding

(b) After adjusting the cross-section, minor bumps in the hinge zone remain

Figure 4.4: Fixing errors appearing after unfolding

If there are sizable changes in bed-thickness after flexural-slip unfolding this indicates that the cross-section is flawed and some revision is necessary before it can be considered balanced. Especially the hinge zones need close examination as to be bed thickness there often tends to look thicker than it really is. See 4.4a for an example of this.

Minor variations in bed-thickness are inevitable due to scale and the way of drawing the cross-section. Very precise cross-sections without slightly uneven beds fall outside the scope of the project.

Line-length Unfolding

The line-length unfolding algorithm works by unfolding a line to an undeformed state represented by a perfectly straight line. The unfolding is performed relative the intersection of the line and a pin. The algorithm works by rotating the limbs of a fold such that the line length is maintained. In essence, it simply converts the deformed horizon to a straight state. No template is required as all lines are unfolded independently of one another (Mov, 2017). Hence bed thickness is not maintained.

The unfolded lengths of the horizon lines in one cross-section should not diverge too much from each other, all should have approximately the same length. The younger formations higher up in folds are usually a little longer. If a cross-section has wildly varying horizon lengths then this indicates that the interpretation is flawed.

Once all the restored cross-sections no longer have unaccountable changes in volume or length they can be considered 'balanced', meaning the interpretation is geologically possible, the 3D modelling can begin.

5

3D Modelling

5.1. Surface Creation

The formation horizon surfaces are spline-interpolated between the cross-section horizon lines. It is key to collect these lines in the right sequence, otherwise Move will create erratic surfaces between the horizons following this wrong order. To guarantee that the surfaces follows the horizon lines as closely as possible the sample density is set to the lowest setting (every 5m).

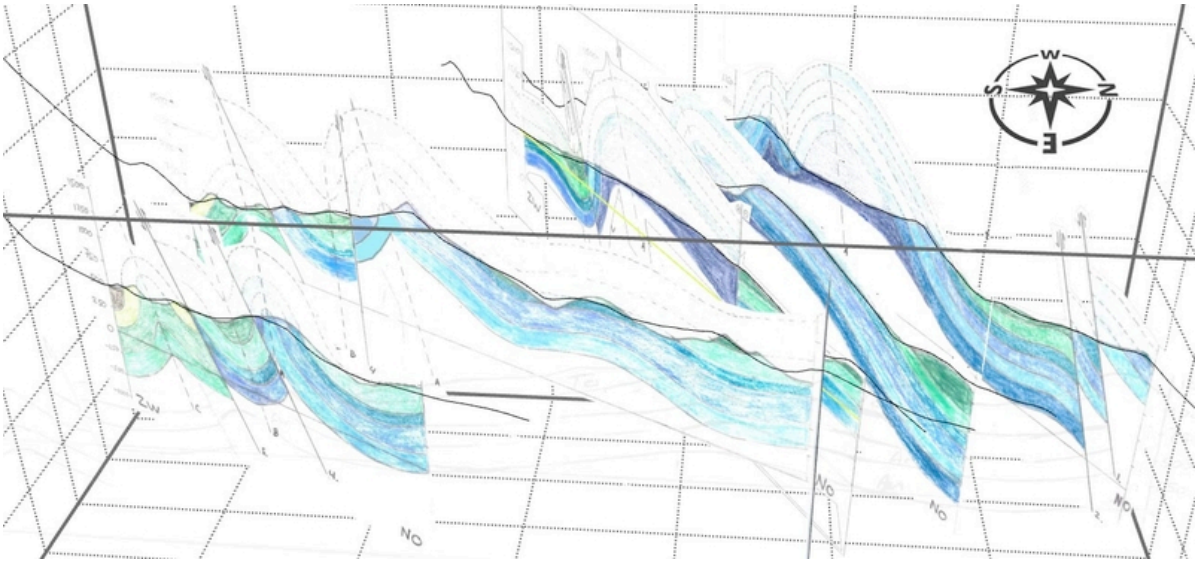

Figure 5.1: Cross-sections imported into Move

Two cross-sections were created exactly along the face of the strike-slip faults, which act as double cross-sections for both the inside and outside of the 'strike-slip triangle'. This because surfaces can not be created from just one line and to ensure that surfaces extend to the face of the strike-slip faults. The 'snap-to surface tool' was tried before but produced unsatisfactory results.

The different orientation of traces causes problems in surface creation. Move simply interpolates between the horizon lines without 'regard' for continuity of of fold orientations and this causes incorrect surface shape. The problem was resolved by splitting formation lines into smaller

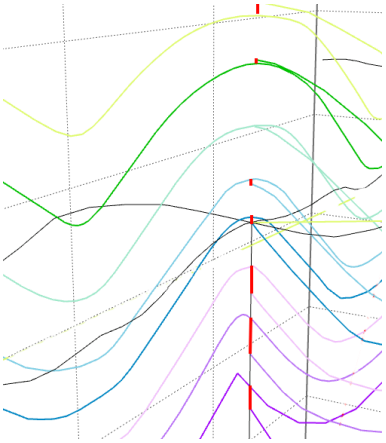

Figure 5.2: Mismatched horizons between sections in 3D. Gaps between horizons indicated with red lines

pieces and creating surfaces between these. This 'patch-work approach; results in more small surfaces. If the horizon lines are at a slightly different altitude from each other then minute gaps between them. This is the trade-off that has to be made for ensuring correct shape.

Because the faults in cross-sections are straight, linear interpolation suffices for creating fault surfaces.

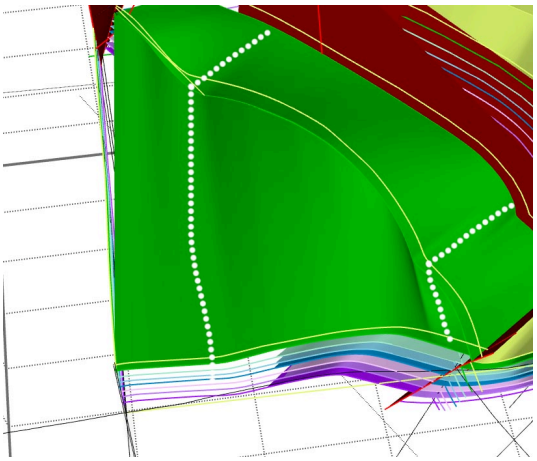

(a) Incorrectly created surface, note the implausible angle in the fold axes, marked with a white dotted line

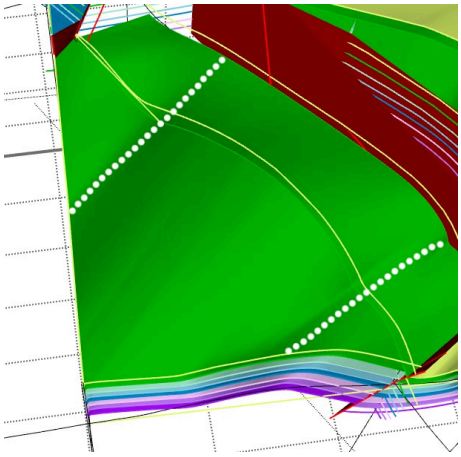

(b) Correctly created surface, with a more probable continuous fold axes

Figure 5.3: Example of surface creation

5.1.1. Spline Interpolation

A spline is a piece-wise polynomial between a pair of tabulated points, but one whose coefficients are determined slightly non-locally. The use of non-local points is to circumvent the lack of smoothness in the interpolated function (C.Vuik, P. Beek, F. Vermolen, and J. van Kan, 2007). In essence this is to prevent surfaces from becoming jagged.

5.2. Moving Faults in 3D

To remove the fault displacement in the 3D model the horizon surfaces are moved along the fault surfaces. Again the fault parallel flow algorithm is used.

Fault parallel works by dividing the fault plane into discrete dip domains where a change in the fault's dip is marked by a dip bisector. Flow lines are constructed by connecting points on different dip bisectors of equal distance from the fault plane. Particles in the hanging wall translate along the flow lines, which are parallel to the fault plane, by the distance between the hanging- and foot wall horizon (Mov, 2017). Fault parallel flow is especially suited for modelling faults from fold and thrust belts like this area. This is a computationally expensive operation and takes a few hours complete.

5.3. 3D Unfolding

This is the final step of restoring the model to its pre-deformational state. 3D Unfolding is performed to validate complex thrust deformations by way of unfolding the rocks and then to translate the unfolded components to their pre-deformational positions. The model is validated if the unfolded rocks can be reassembled to form a coherent geometry, without gaps or overlaps.

Once again flexural-slip unfolding is used, so the same principles described in chapter 5 for 2D-unfolding hold. The flexural slip algorithm allows unfolding while preserving the thickness between surfaces, bed thickness variations, and line-length of the template bed in the unfolding direction. This makes it very suited for unfolding fold-thrust belts like this area.

A pin plane is positioned parallel to the hinge line of the fold where shear has not occurred across the axial surface. In contrast, the unfolding plane should be placed perpendicular to the hinge line (Mov, 2017). The surfaces are all moved to a fixed datum.

Four different pin- and unfolding planes orientations were used to unfold the area. These correspond to each 'segment' bounded by faults. In figure 5.4 the areas of different unfolding planes are illustrated.

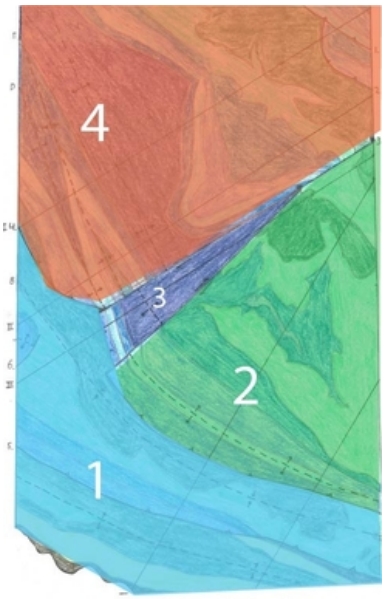

Figure 5.4: Four sections for which different unfolding plane orientations were used

6

Results

6.1. Cross-Sections

Cross-Section I

Figure 6.1: Legend for digitized cross-sections formations

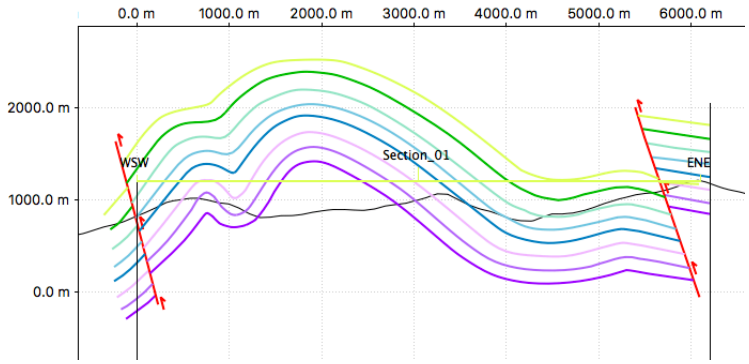

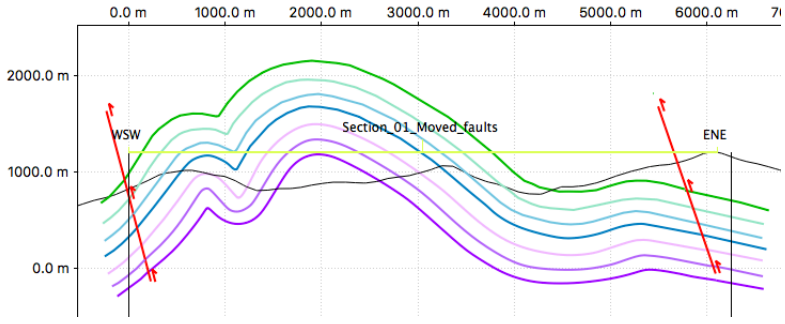

Figure 6.2: Fault displacements removed

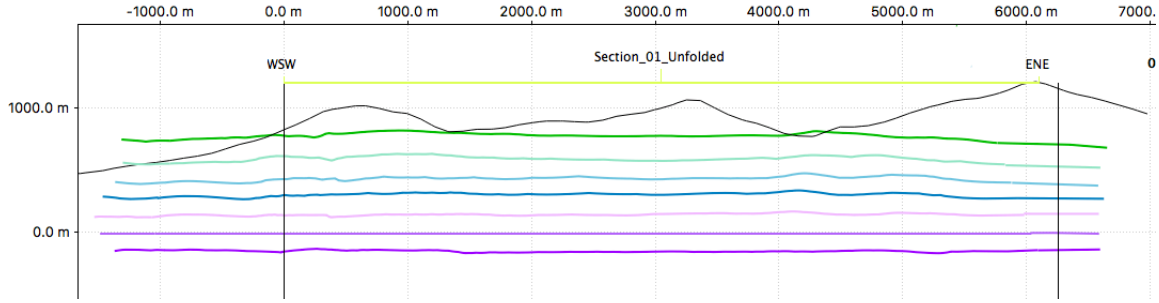

Figure 6.3: Flexural slip unfolded

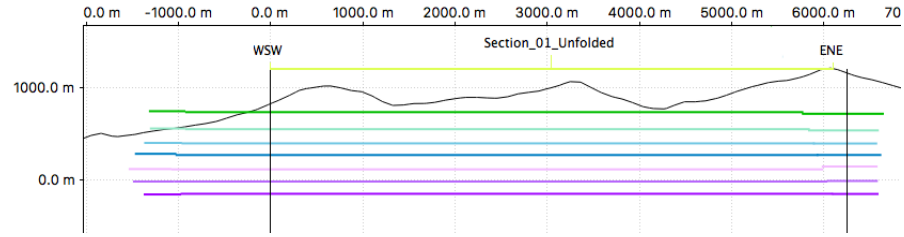

Figure 6.4: Line length unfolded

Cross-Section II

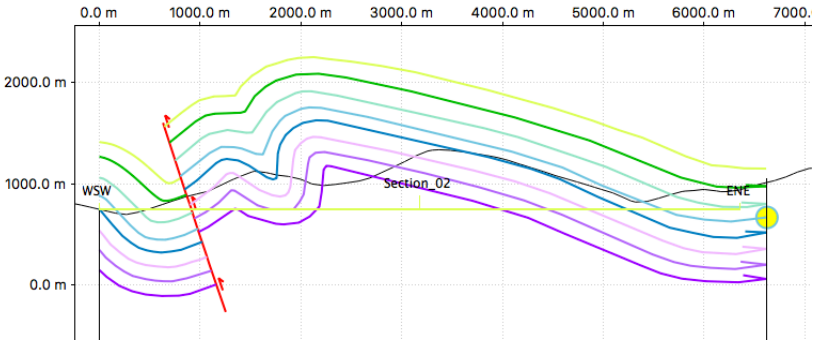

Figure 6.5: Digitized cross-section

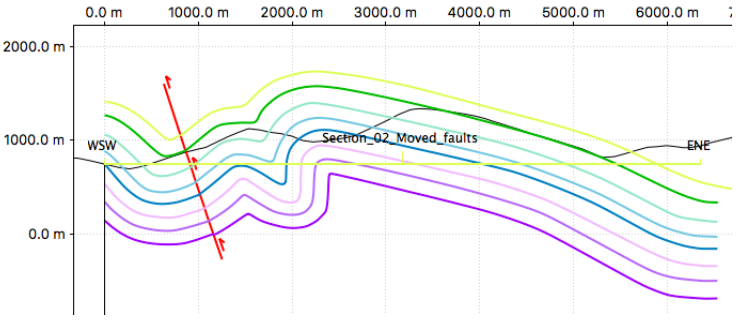

Figure 6.6: Fault displacements removed

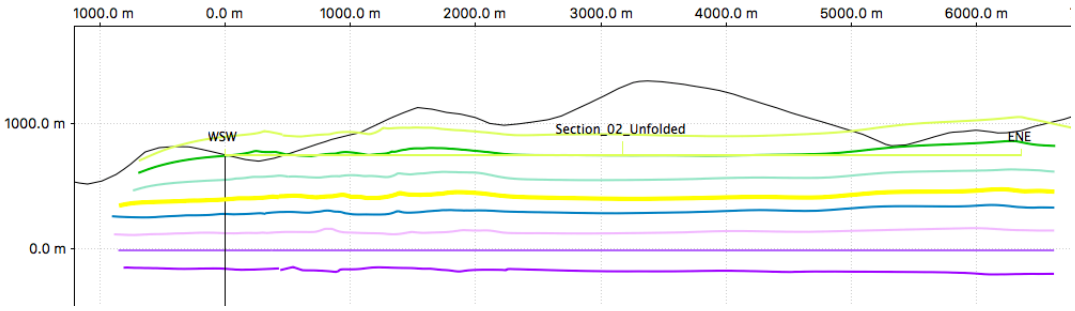

Figure 6.7: Flexural slip unfolded

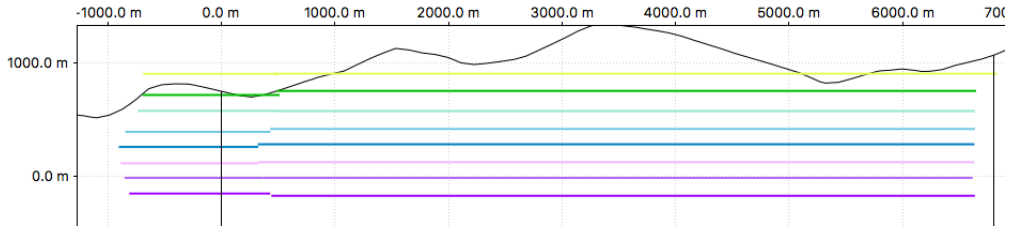

Figure 6.8: Line-length slip unfolded

Cross-Section III

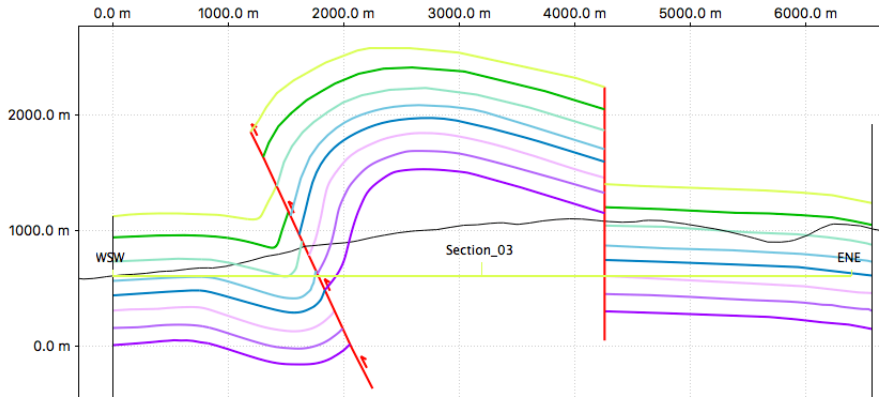

Figure 6.9: Digitized cross-section

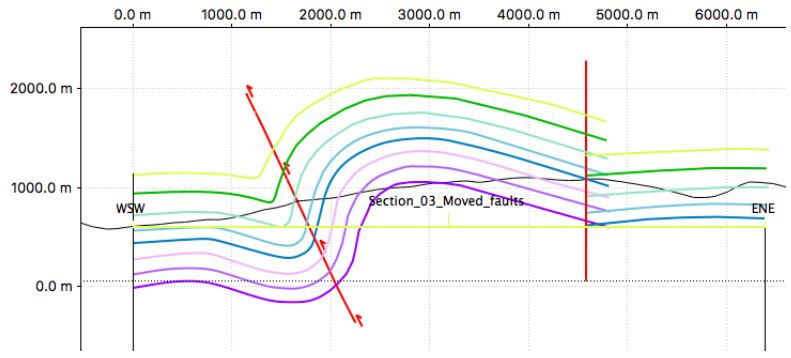

Figure 6.10: Fault displacements removed

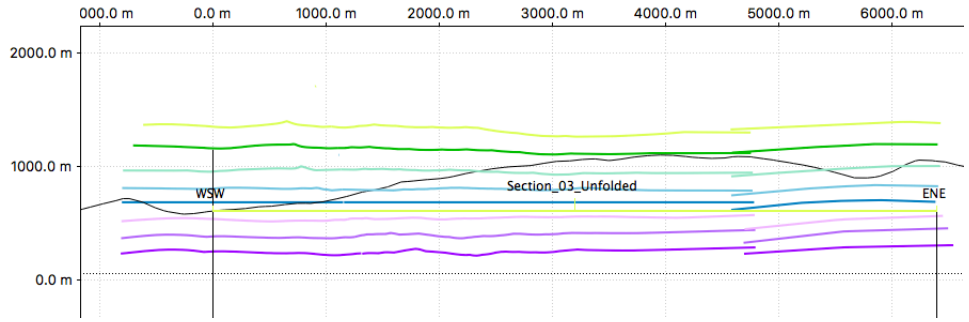

Figure 6.11: Flexural slip unfolded

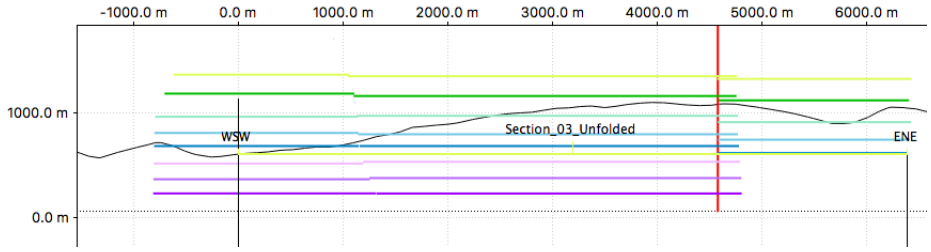

Figure 6.12: Line length unfolded

Cross-Section IV

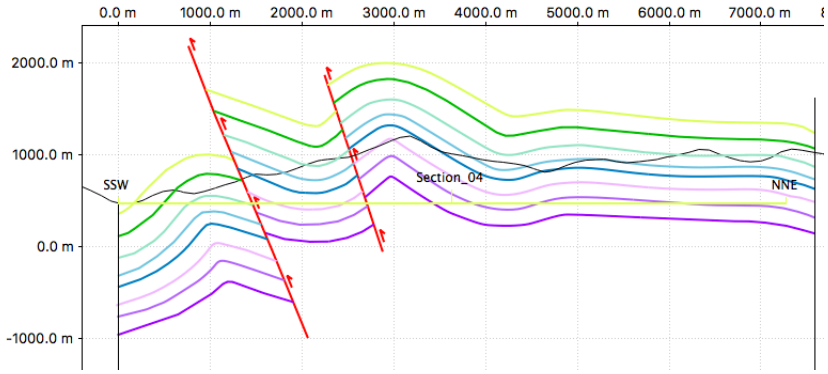

Figure 6.13: Digitized cross-section

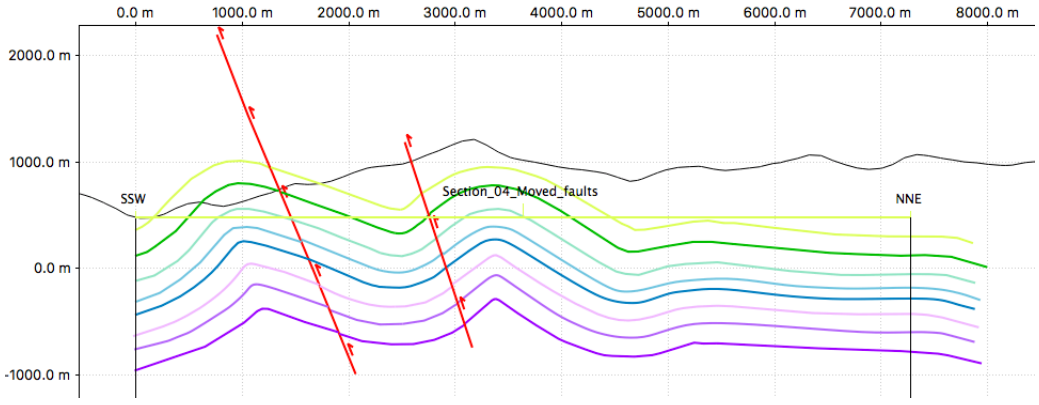

Figure 6.14: Fault displacements removed

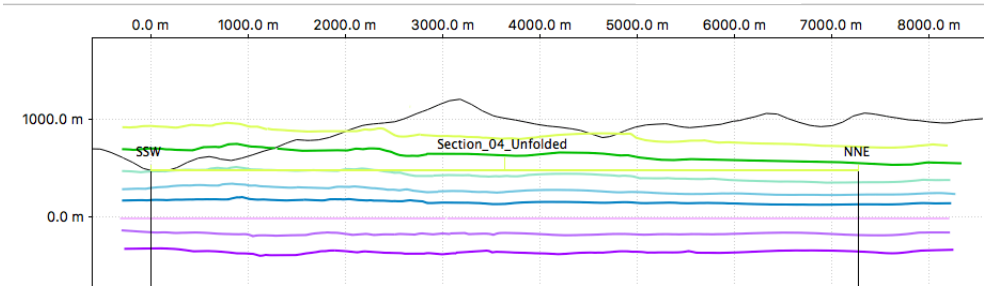

Figure 6.15: Flexural slip unfolded

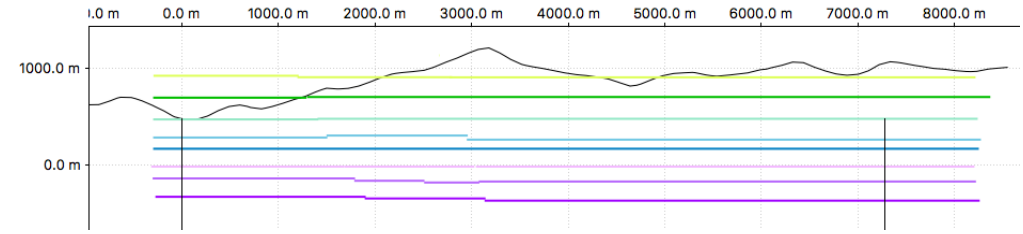

Figure 6.16: Line length unfolded

Cross-Section V

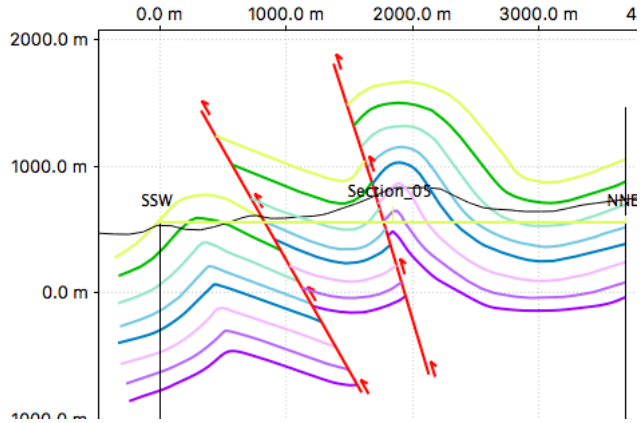

Figure 6.17: Digitized cross-section

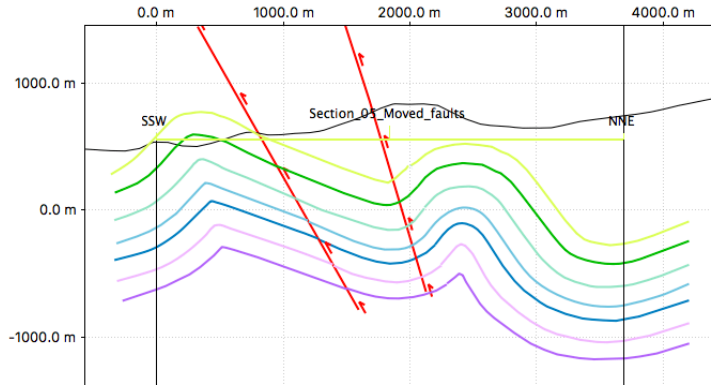

Figure 6.18: Fault displacements removed

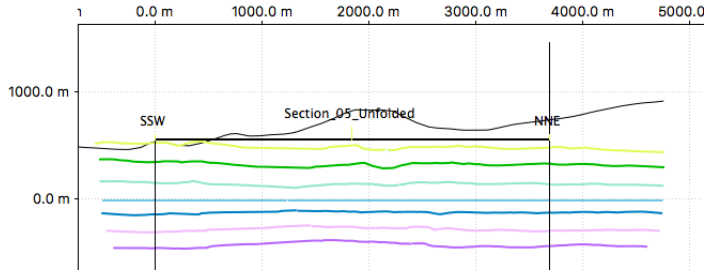

Figure 6.19: Flexural slip unfolded

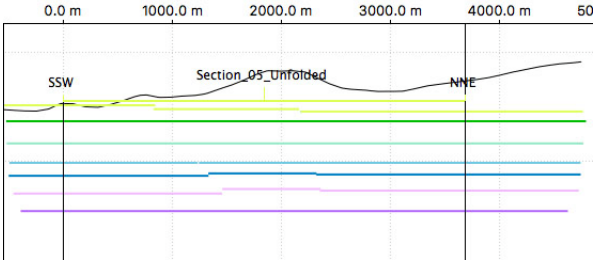

Figure 6.20: Line-length unfolded

Cross-Section North

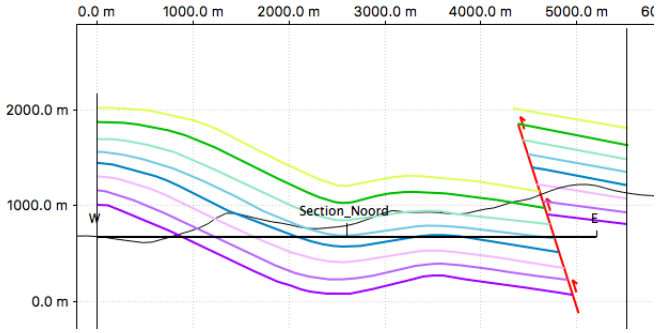

Figure 6.21: Digitized cross-section

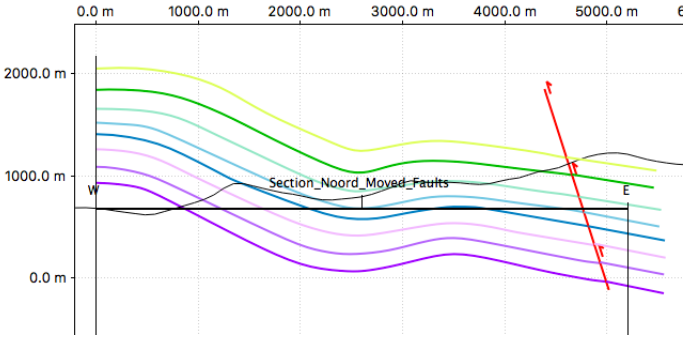

Figure 6.22: Fault displacements removed

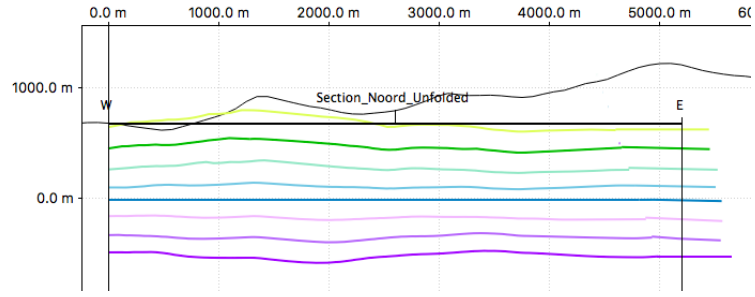

Figure 6.23: Flexural slip unfolded

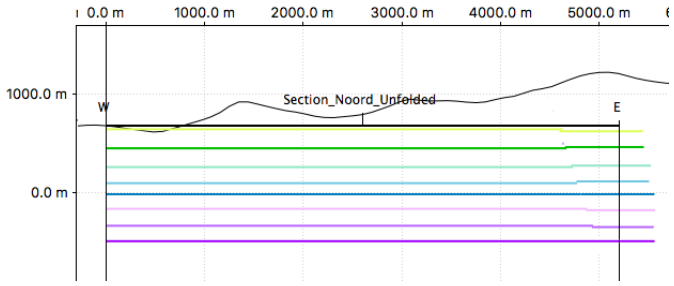

Figure 6.24: Line length unfolded

Cross-Section East

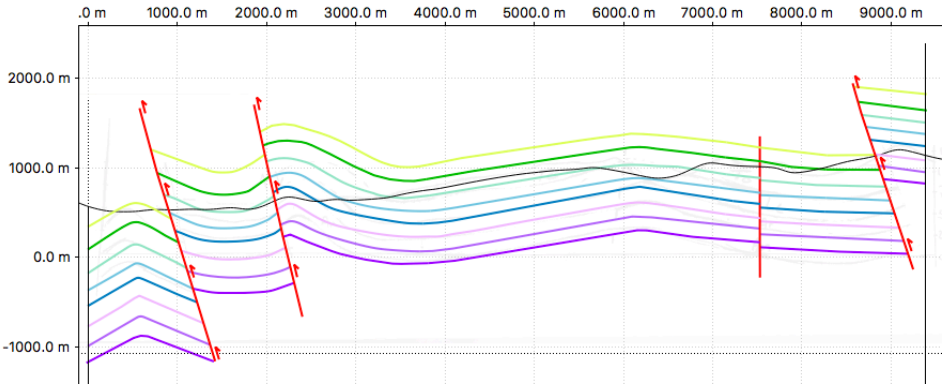

Figure 6.25: Digitized cross-section

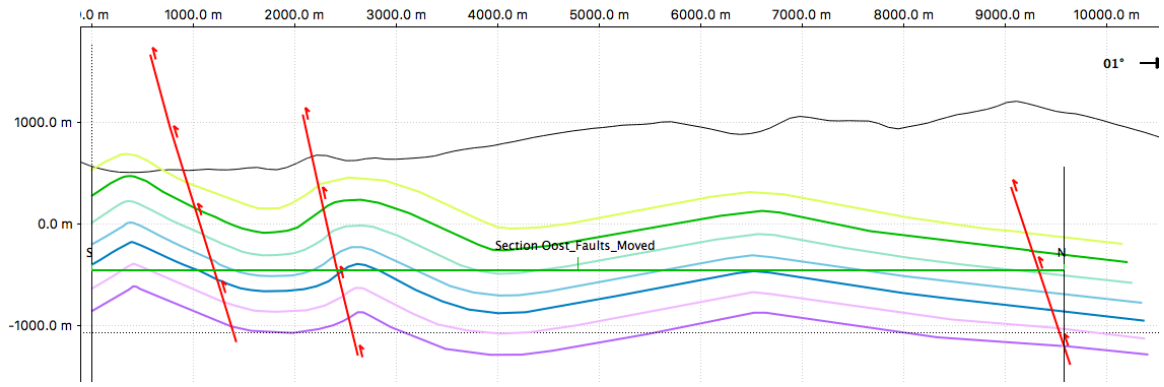

Figure 6.26: Fault displacements removed

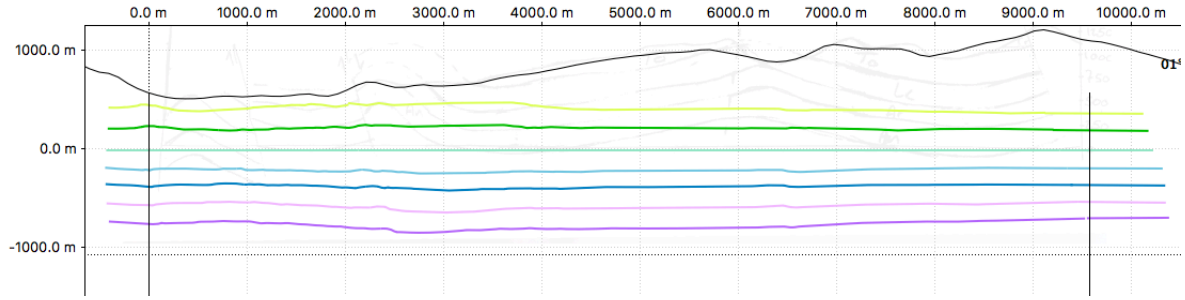

Figure 6.27: Flexural slip unfolded

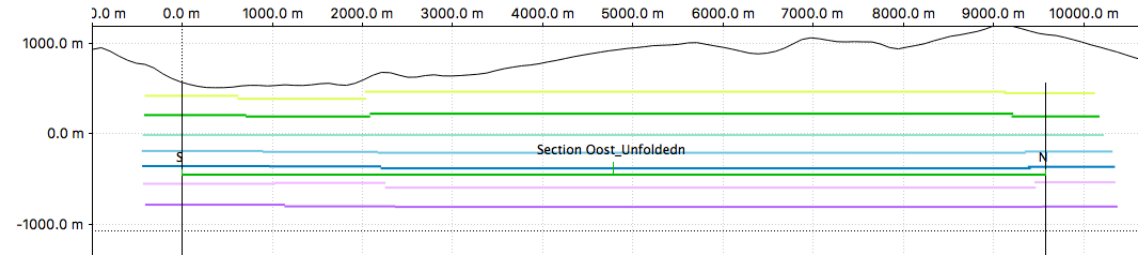

Figure 6.28: Line length unfolded

Cross-Section West

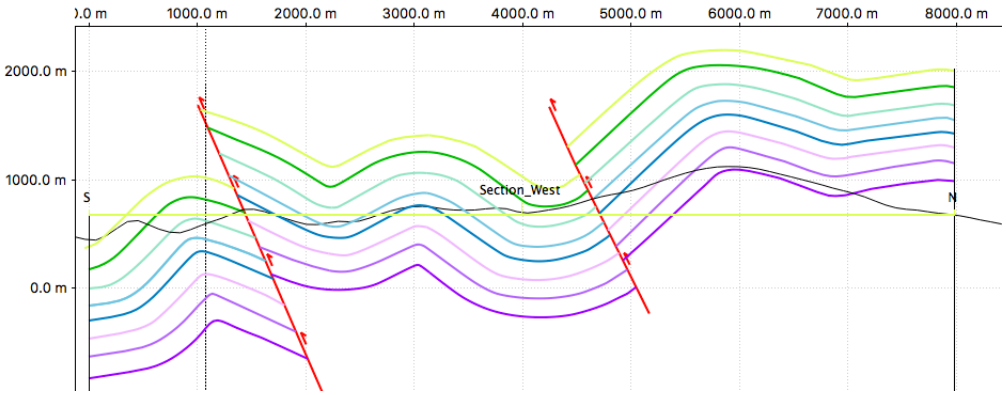

Figure 6.29: Digitized cross-section

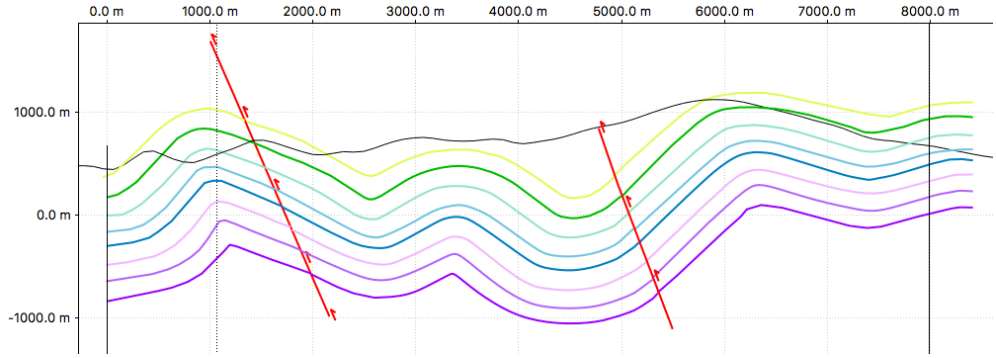

Figure 6.30: Fault displacements removed

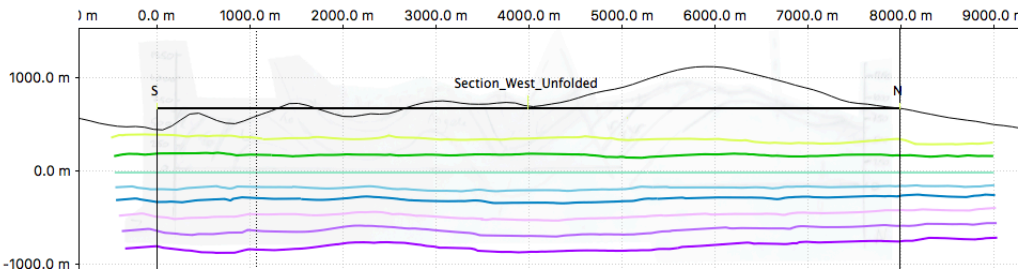

Figure 6.31: Flexural slip unfolded

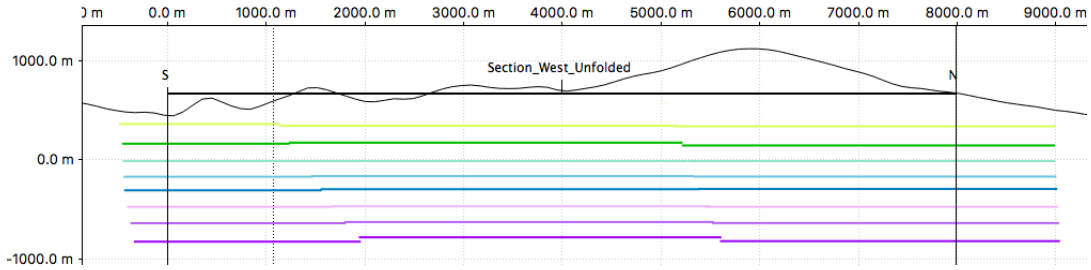

Figure 6.32: Line length unfolded

6.1.1. Quality Control

Table 6.1: Rounded line-lengths of cross-sections before and after restoration

Cross-section	Deformed (m)	Restored (m)	Shortening %
I	6400	8050	20.5%
II	6600	7580	12.93%
III	6580	7400	11.08%
IV	7600	8580	11.42%
IV	3900	5200	25.00%
North	9400	10800	12.96%
East	8000	9450	15.34%
West	5520	6030	8.46%

The average shortening per cross-section amounts to 14.71 %.

It's apparent that horizon lengths tend to diverge more in cross-section with more folds. This is because horizons farther 'at the bottom of the fold' are shaped differently than those above.

Cross-section V, with shortening of 25% deviates most from the average. This might indicate the fold E is constructed too convex in this cross-section. The difference between in percentage shortening cross-section I and II is probably because cross-section I also includes reverse-fault 1.

6.2. 3D Model

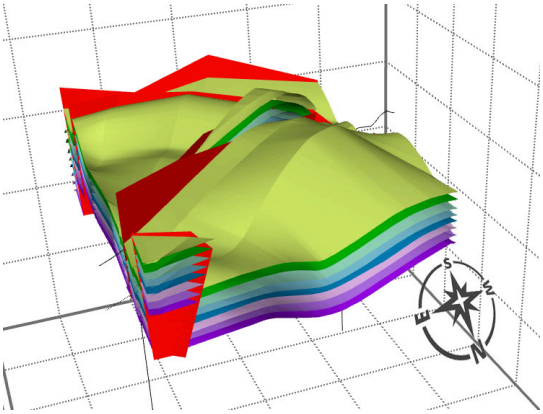

(a) View from north

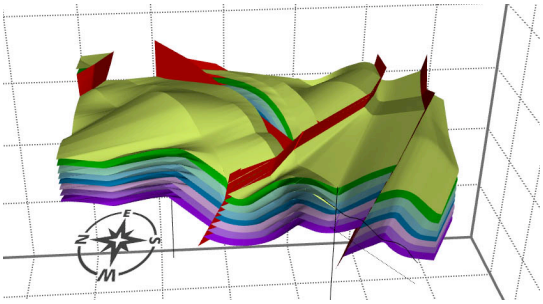

(b) View from west

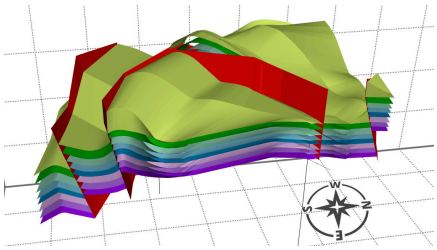

(c) View from east

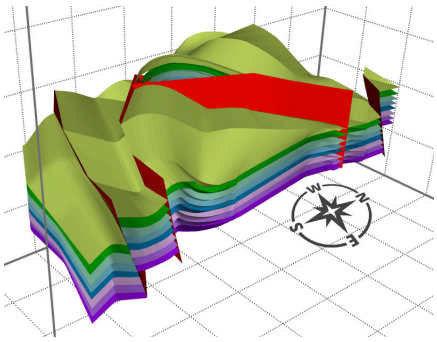

(d) View from southeast

Figure 6.33: 3D Model with formation horizon surfaces

6.2.1. 3D Moved Faults

Most horizons fit quite nicely with each other after the fault displacements are removed. The surfaces west of the long strike-slip fault are moved up for some reason. Various combinations of different hanging- or footwall surfaces and settings have been tried but the problem remains.

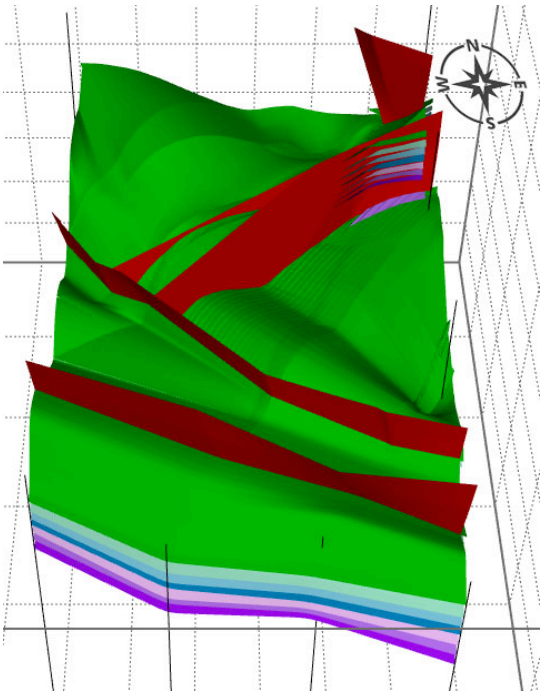

(a) View from south, above

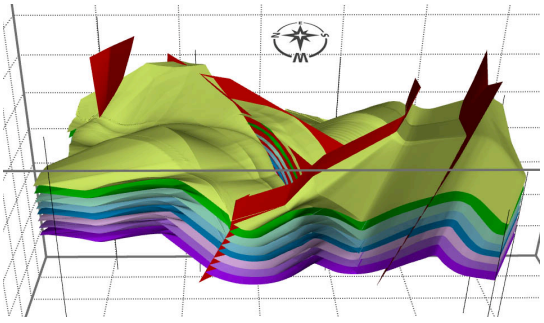

(b) View from west

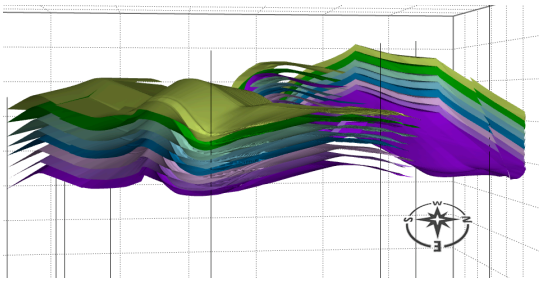

(c) View from east

Figure 6.34: Model after removing of fault displacements

6.2.2. 3D Unfolded

Unfolding all surfaces can take up to 5 hours to complete so only the Tithonian horizon surfaces have been unfolded. This formation was chosen because of its hardness, therefore it does not deform viscously.

The result has some overlapping surfaces and some gaps between surfaces requiring manual movement and rotation of areas to decrease misfit. Before manual movement, there is 30.07% misfit of horizon area. After moving and rotating surfaces, the misfit percentage was reduced to 25.17%. This still seemed high, but Move mistakenly counts the area between the small protrusion in the northwestern corner and northeastern corner as a gap. When this gap is ignored the misfit percentage is reduced even further to 18.6 %.

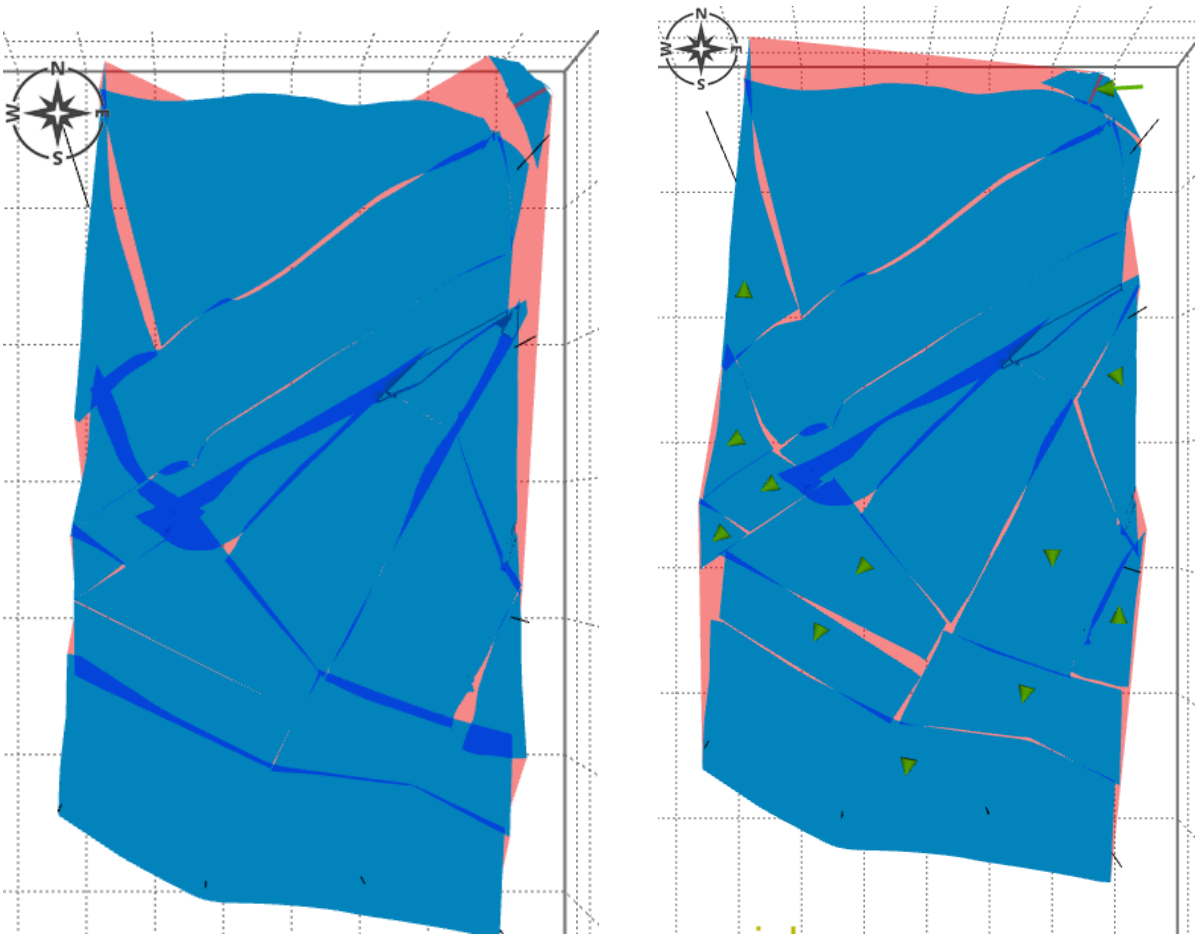

(a) Before manual movement, gaps indicated in red and overlap in blue

(b) After movement and rotation of surfaces, green arrows indicate direction of movement

Figure 6.35: 3D unfolding of Tithonian horizon surfaces

The biggest offender in overlapping surfaces is the 'strike-slip triangle' south-east of Montagne de Banne, indicating that this fold was constructed too long and convex. This is hardly surprising as mostly Terres Noires surfaces there, which has no layers with measurable orientation, so the fold shape is estimated.

The gap directly south of fault 4 indicates that the dip of this fault is too steep, and therefore .

The overall decrease in surface area due to deformation is 8.2 km^2 or 14.3 %. Note that overlapping surfaces do not contribute to this increase. This corresponds closely with the average shortening found for the cross-sections.

6.2.3. New Geologic Map

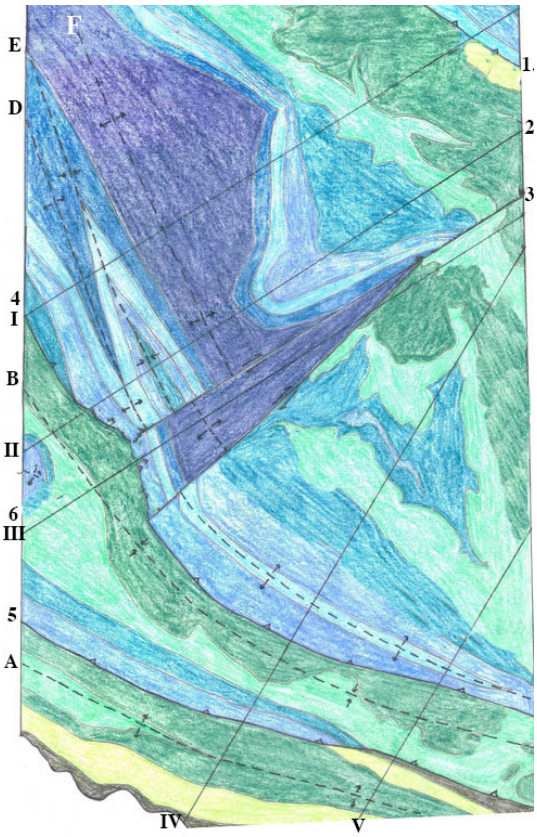

Figure 6.36: Adjusted geologic map

7

Conclusion & Recommendations

7.1. Discussion

There are many terms of uncertainty in constructing a three-dimensional geological model. First, the 1:25 000 scale means that small inaccuracies in scale drawings translate to deviations of dozens of meters in the model. Second, during modeling many assumptions and simplifications have to be made. For example, it is assumed that formation thickness is constant. Another assumption is that the folding occurred completely before faults formed in order to remove the effects of deformation sequentially. But it more probable that these processes happened partially simultaneously.

Reverse-faults in fold-and-thrust belts usually have and a dip of around 45°. This point to

Second, field data is scarce in some parts of the area, requiring extrapolations to be made from the parts where field data is available. Third, these two-dimensional cross-sections are interpolated to three-dimensional structures, introducing even more uncertainty. Third, arguably some amount of confirmation bias has crept into field observations and the interpretation skewing the model to fit the ideas in the mind of the interpreter.

All of obstacles can lead to a model with unaccounted changes in volume, thickness or length of formations. It is important to think about what the issues encountered represent and whether these are workflow based or interpretation based.

At the start of this project, I had a lot of confidence in the interpretation made during the field work and assumed modeling and restoring it in 3D would be a fairly straightforward task. Along the way more and more doubts arose about the existing cross-sections and geological map.

While most of the flaws were resolved, there are still some debatable parts. It is suspected that formation thicknesses varies a little too much in the model. Especially the Barremian formation, since not much of it surfaces. Another area I'm not sure about is the configuration of formations in the eastern part of the area since field data here was limited.

Constructing balanced cross-sections proved to be harder than expected. Just when all cross-sections were thought to be well balanced, the first 3D surfaces were created and flaws emerged. At this point, it became clear that for an interpretation to be verified a 3D model needs to be built. The most notable flaw emerging was disparate horizon depths between cross-sections. This required some cross-sections to be overhauled significantly and therefore also balanced again. This process of revising, rebalancing and then checking the cross-sections in 3D could be done repeatedly and new flaws seemed to arise each time. Revision proved rather time-consuming and due to time constraints the cross-sections had to be considered good enough at a certain point. Ultimately the model remains an approximation, not an exact replica of in-situ conditions.

Some errors introduced in restoration could not be resolved, like erratic movement of surfaces after removing faults displacements. I suspect this is a side-effect of the algorithm used. Others issues, like the sizable overlap after 3D unfolding, are decidedly interpretation based.

7.2. Conclusion

The purpose of the constructing and restoring was to gain an understanding of the tectonic history and check whether the former interpretation was geometrically valid. Again, it is important to note that

balanced does not axiomatically imply that the model accurately reflects the true situation; only that the model is geologically viable.

The average shortening of cross-sections was 14.71%.

The increases in surface area after removing fault displacement in the 3D model was 14.3 %.

The misfit after unfolding of the Tithonian horizon surfaces was 18.6 %. The total decrease in surface area due to deformation is 8.2 km^2 or 14.3%.

The end result is a geologically feasible model within the constraints of limited field data.

7.2.1. Differences from Old Interpretation

All main geologic structures were already recognized in the previous interpretation. The changes are all relatively small.

First, there is, in fact, no fault in the northeastern corner near the village Poët-en-Percip. Therefore there is also no Tithonian and Kimmeridgian surfacing north of this supposed fault. Instead Hauterivian and a small strip of Barremian surface here.

In the area southeast of Montagne de Banne (around Mt de la Bohémienne) less Valanginian surfaces than assumed before. For that much Valanginian to surface there the formation would have to be much thicker. In addition, satellite images show no badlands here and thus disparage the idea that Valanginian surfaces here.

The reverse-fault in the middle of the area (fault 4) is changed into one continuous fault instead of being 'interrupted' by the strike-slip faults. Because there is no evidence that the strike-slip faults cut through the reverse-fault.

In most cross-sections, the fold hinge zones required adjustments in order to make the model balanced. The most prominent example of this is the attenuation of the fold angles (folds D & E) in cross-section II.

The anticline with Tithonian on top intersecting the western boundary around 'Bois de la Draye' was thought the be an anticline terminating on the end of a fault (fault 6). But is really the tail end of a dipping anticline.

The fold in the 'strike-slip triangle' (fault 3) was constructed too long and convex as evidenced by the significant overlap of this area after 3D unfolding. Please see figure **??** for the improved geological map of the area.

7.3. Recommendations

Being very meticulous in the early stages of cross-section construction pays off later in the modeling process. For instance, checking the altitude of horizons between adjacent cross-sections would have saved a lot of work later on. Cutting corners will invariably produce graver errors later in the process.

Profile traces should have been traced in the DEM with exact UTM coordinates. They were traced in the Digital Elevation Model by eye, using the draped geological maps as a guide. The draping of the image over the DEM warps the image and thereby distorts the 'exact' locations of the profile lines.

Because it is assumed that formation thicknesses are constant in this area, thicknesses should have been maintained more between sections. With varying lengths of cross-sections, different zoom levels were used in the Move software during construction. Therefore sometimes not enough attention was paid to scale and caused certain formations to be constructed a bit too thick or thin in some cross-sections.

Cross-sections should have been constructed roughly parallel to each other. As Move produces irregular surfaces when multiple cross-sections are different angles to each other as shown in figure 5.3a.

Additional cross-sections would have been helpful. However, constructing and validating many extra cross-sections would have been prohibitively time consuming for this thesis. Field observations represent the most direct and important source of information, accordingly a new visit for data would surely improve the model.

For future studies, it would be advised to keep an eye on the big picture, instead of focusing on individual cross-sections. In short, check whether what is made in one cross-section is consistent with the complete model. In future studies, effects of compaction and erosion can be considered in constructing a model.

8

Acknowledgements

The author would like to thank his supervisor Jan Kees Blom for his assistance throughout the thesis and for turning many 'short' questions into long and insightful discussions. Jan Kees provided many valuable tips, colourful analogies and clarifying examples throughout the modeling process. Especially the Google Earth and Streetview examples proved to be very useful. Midland Valley Ltd. is thanked for their generous offering of an academic license for the Move software suite.

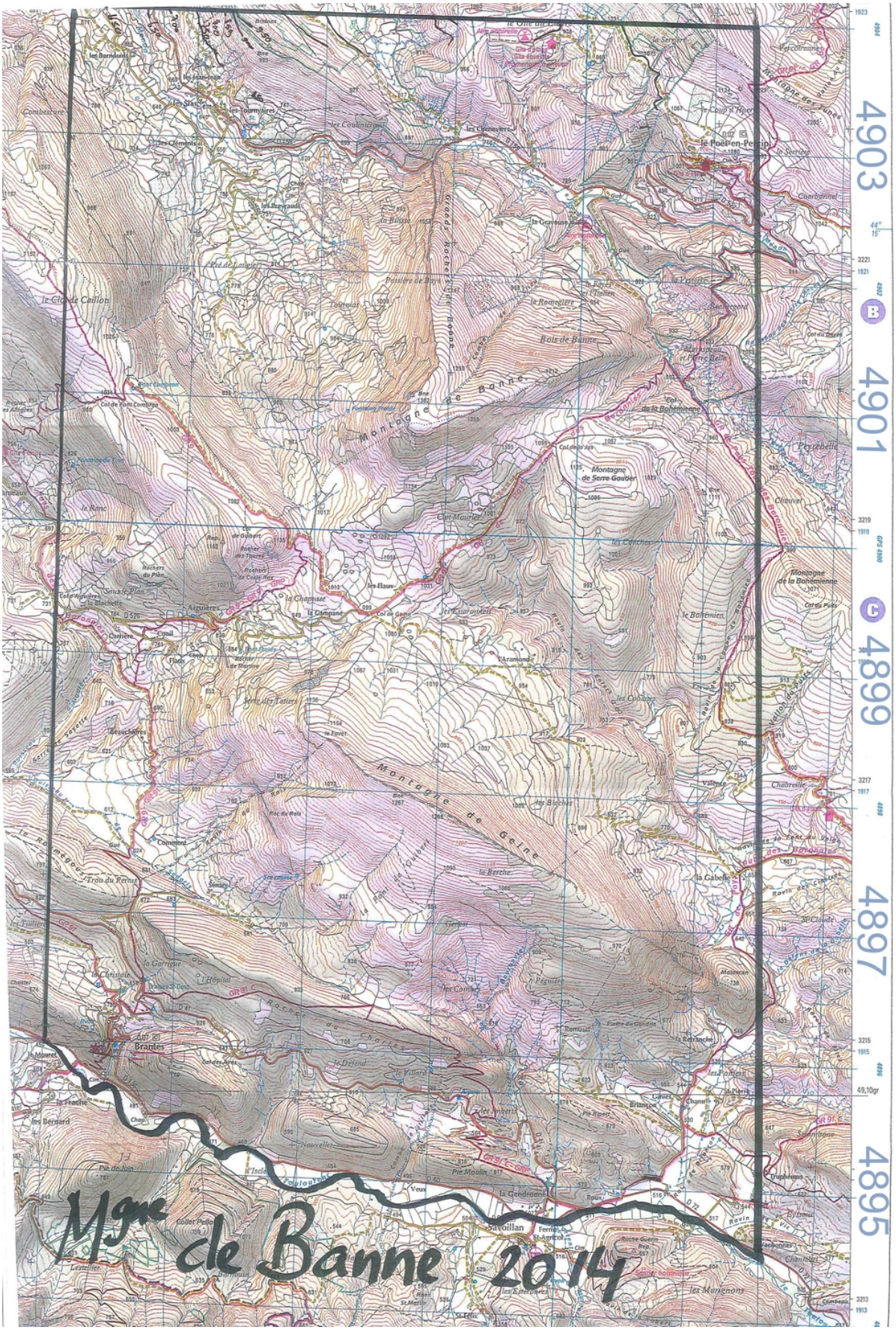

Figure 1: Topographic map of the Montagne de Banne area

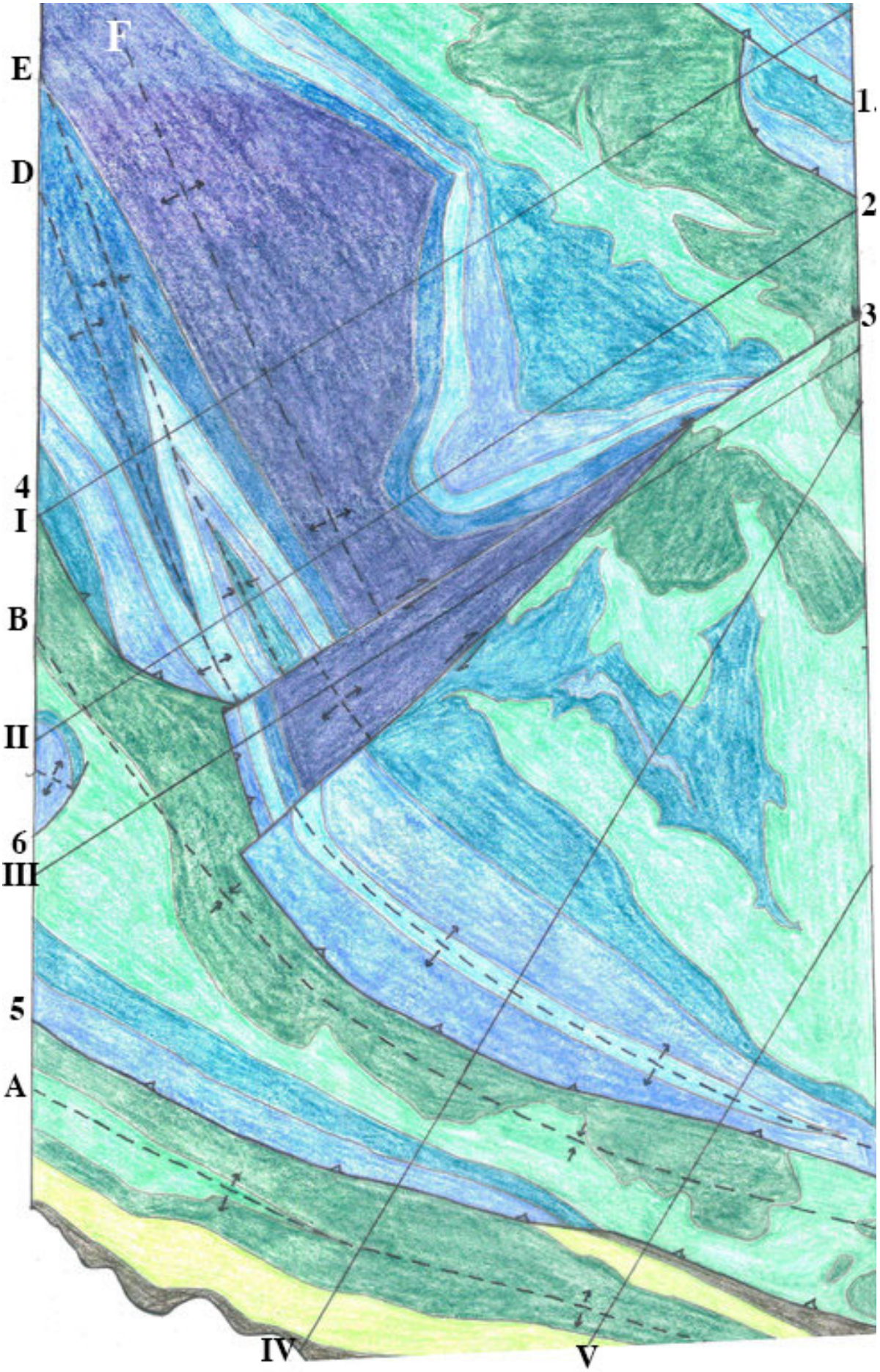

Figure 2: Geological Map constructed for 2015 fieldwork

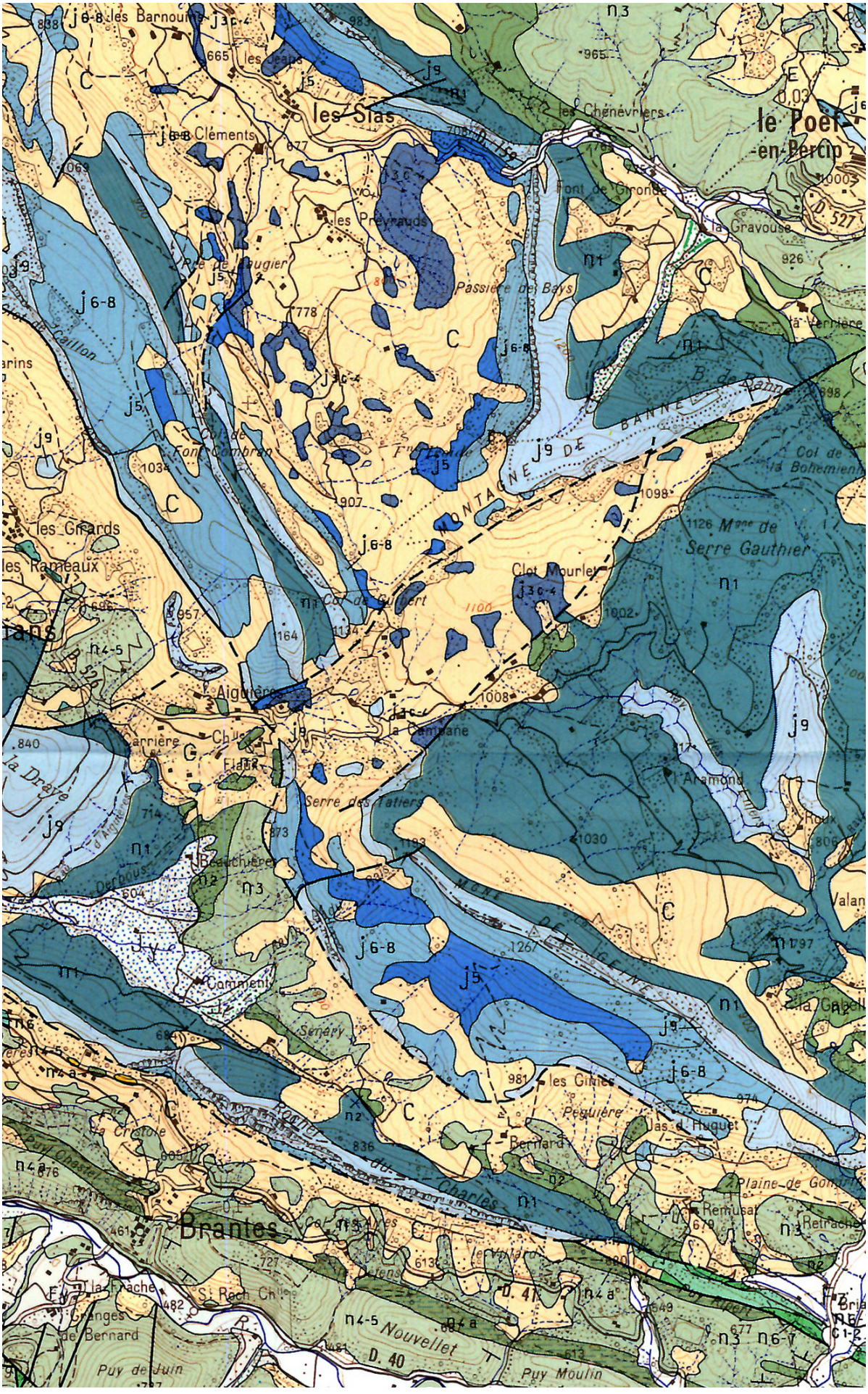

Figure 3: Geological map of studied area. Extracted from BGRM's Vaison-la-Romaine geological map sheet no. 3140

Bibliography

Midland valley exploration ltd move suite description, https://www.mve.com/software/move (2017), accessed: 2017-09-15.

M. Lemoine and T. Bas, *The continental margin of the mesozoic tethys in the western alps,* Marine and Petroleum Geology **3** (1986).

M. Wilpshaar et al, *Early cretaceous sedimentary and tectonic development of the dauphinois basin (se france),* Cretaceous Research **18**, 457 (1997).

C. Ranging, X. Le Pichon, Y. Hamon, N. Loget, and A. Crespy, *Gravity tectonics in the se basin (provence, france) imaged from seismic reflection data,* Bull. Societé géologiquel **6**, 503 (2010).

Courjault et al, *Detailed anatomy of a deep-water carbonate breccia lobe (upper jurassic, french sub-alpine basin),* Sedimentary Geology **238**, 156 (2011).

P. Joseph et al, *Submarine valleys evidence lower cretaceous tilted block activity in the vocontian basin,* Sedimentology **2**, 1031 (1989).

L. Bombardiere and G. Gorin, *Stratigraphical and lateral distribution of sedimentary organic matter in upper jurassic carbonates of se france,* Sedimentary Geology **132**, 177 (2000).

Greselel & Pettet, *Sea-level reconstructions from the peri-vocontian zone (south-east france) point to valanginian glacio-eustasy,* Sedimentology **57**, 1640–1684 (2010).

Boulila et al., *Milankovitch and sub-milankovitch forcing of the oxfordian terres noires formation (se france) and global implications,* Basin Research **22**, 717–732 (2010).

J. Breheret and B. H.J., *Barite concretions as evidence of pauses in sedimentation in the marnes bleues formation of the vocontian basin (se france),* Sedimentary Geology **130**, 205–228 (2000).

Micarelli et al., *Influence of p/t conditions on the style of normal fault initiation and growth in limestones from the se-basin, france,* Journal of Structural Geology **27**, 1577 (2005).

E. Mattioli, S. Gardin, and B. Pittet, *Guidebook for the post-congress fieldtrip in the Vocontian Basin, SE France* (Notebooks on Geology, 2008).

Boulila et al., *Anatomy of ancient passive margin slope systems: Aptian gravity-driven deposition on the vocontian palaeomargin, western alps, south-east france,* Sedimentary Geology **324**, 1 (2015).

C. Colombié and A. Strasser, *Depositional sequences in the kimmeridgian of the vocontian basin (france) controlled by carbonate export from shallow-water platforms,* Geobios **26**, 675–683 (2004).

Leonide et al, *Relation between stratigraphic architecture and multi-scale heterogeneities in carbonate platforms: The barremian–lower aptian of the monts de vaucluse, se france,* Sedimentary Geology , 23 (2012).

G. Fries and O. Parize, *Anatomy of ancient passive margin slope systems: Aptian gravity-driven deposition on the vocontian palaeomargin, western alps, south-east france,* Sedimentology **50**, 1231–1270 (2003).

Koessler et al., *Magnetic records of climatic cycles from mid-cretaceous hemipelagic sediments of the vocontian basin, se france,* Cretaceous Research **22**, 321 (2001).

P. N. Froelich, G. P. Klinkhammer, and M. L. Bender, *Early oxidation of organic matter in pelagic sediments of the eastern equatorial atlantic: suboxic diagenesis,* Geochimica et Cosmochimica Acta **44**, 1075–1090 (1979).

P. Monier, G. Truc, and J. Flandrin, *Carte geologique de le france a 1/50 000 vaison-la-romaine sheet no. 3140,* (1987).

G. Stampfli, G.M. Borel and R. Marchant, *Western alps geological constraint on western tethyan reconstruction,* Virtual Explorer **7**, 75–44 (2002).

J. Coward and Dietrich, *Structural and sedimentary records of the oligocene revolution in the western alpine arc,* Alpine Tectonics **45**, 1 (1989).

Dumont et al., *Structural and sedimentary records of the oligocene revolution in the western alpine arc,* Journal of Geodynamics **56** (2011).

John W.F. Waldron, *University of alberta: Structural geology and tectonics: Foreland thrust and fold belts,* .

Haakon Fossen, *Structural Geology* (Cambridge University Press, 2010).

J. Ziesch, *Strain associated with the fault-parallel flow algorithm during kinematic fault displacement,* Mathematical Geosciences **46**, 58–73 (2014).

C.Vuik, P. Beek, F. Vermolen, and J. van Kan, *Numerical Methods for Ordinary Differential Equations* (VSSD, 2007).